Depositional Age, Provenance Characteristics and Tectonic Setting of the Ailaoshan Group in the Southwestern South China Block

JI Lei[1, 2, *], LIU Fulai[1, 2], WANG Fang[1, 2] and TIAN Zhonghua[1, 2]

[1] *Institute of Geology, Chinese Academy of Geological Sciences, Beijing 100037, China*
[2] *Key Laboratory of Deep-Earth Dynamics of Ministry of Natural Resources, Beijing 100037, China*

Abstract: The depositional and metamorphic ages and provenances of the Ailaoshan (ALS) Group in the Ailaoshan-Red River (ALS-RR) shear zone, southwestern South China Block (SCB), were investigated to constrain the tectonic history of the southwestern SCB. In this study, we use petrology, geochemical analysis, zircon cathodoluminescence imaging and U-Pb geochronology to analyse samples of quartzite, garnet-bearing two-mica schist and metapelite. The age spectra of detrital zircon grains from these metasediments show two dominant age peaks at 550–424 Ma and 876–730 Ma and two subordinate peaks at 970–955 Ma and ~2450 Ma. The youngest peak, corresponding to the early Palaeozoic, accounts for more than 20% of the total dates and constrains the deposition of the ALS Group to the Palaeozoic rather than the Palaeoproterozoic as traditionally thought. Moreover, two peaks of metamorphic ages corresponding to the Permo-Triassic and Cenozoic were also identified, and these ages document the tectonothermal events associated with the Indosinian collision between the Indochina Block and the SCB and the Himalayan collision between the Indian and Asian plates. Geochemical data suggest that the provenances of the ALS Group were dominated by continental arc and recycled metasedimentary rocks. The comparison of probability density distribution plots of the detrital zircon U-Pb age data indicates that the Neoproterozoic detritus in the ALS Group was probably derived from the arc-related Neoproterozoic intrusive bodies in the northwestern and southwestern SCB. Furthermore, the early Palaeozoic detritus might have been sourced from eroded early Palaeozoic strata and magmatic plutons in Cathaysia and volcanic rocks in the western Indochina Block.

Key words: detrital zircon, depositional age, provenance, Ailaoshan Group, South China Block

Citation: Ji et al., 2019. Depositional Age, Provenance Characteristics and Tectonic Setting of the Ailaoshan Group in the Southwestern South China Block. Acta Geologica Sinica (English Edition), 93(6): 1687–1710. DOI: 10.1111/1755-6724.14283

1 Introduction

In the southwestern margin of the South China Block (SCB), the Red River fault and the Ailaoshan (ALS) fault define a distinguishable crustal-scale strike-slip shear zone (the Ailaoshan-Red River (ALS-RR) shear zone), which accommodated the energy and material adjustment of the India-Asian collision during the early Cenozoic (Tapponnier et al., 1982, 1990; Zhong et al., 1990; Liu et al., 2012; Zhang et al., 2012, 2017). Vast metasedimentary rocks (commonly referred to as the ALS Group) are present in the ALS-RR shear zone and preserve a record of the sedimentation and metamorphism associated with the evolution of the SCB (Zhong et al., 1998; Liu et al., 2013). The depositional ages and provenances of the metasedimentary rocks in the ALS Group may supply constraints for better understanding the tectonic evolution of the SCB. Due to widespread weathering and vegetation, the depositional age of the ALS Group remains poorly constrained, although it has been proposed that the ALS Group represents a counterpart of the Dahongshan Group to the east, which was confirmed to belong to Paleoperoterozoic by volcanic intercalation (Bureau of Geology and Mineral Resources of Yunnan Province, 1990; Greentree and Li, 2008). In the last two decades, most of the detrital zircon analyses focused on Neoproterozoic-Silurian strata in the central or southeastern SCB (Wang et al., 2010; Yao et al., 2011; Yao et al., 2014, 2015; Xu et al., 2012b, 2013; Chen et al., 2016; 2018; Wang et al., 2018). In contrast, little research has been published on the southwestern SCB, especially the ALS Group. In addition, as a result of the multiple tectonothermal events in this high-strain region, the ALS Group exhibits significant discrepancies in both depositional age and sedimentary provenance, and three distinct views have been proposed. (1) Based on regional stratigraphic correlations, lithologic assemblages, structural relationships, and Sm-Nd isochronal ages, the ALS Group has been traditionally considered to have formed in the Palaeoproterozoic and constitute the basement of the SCB (BGMRY, 1990; Zhai et al., 1990; Zhong et al., 1998). (2) Chen et al. (1991) reported that microfossils of the plants *Trachypeoridium sp* and *Glopheus sp* occurred in the Lower ALS Group (Xiaoyangjie Formation) and concluded that the

* Corresponding author. E-mail: jileicags@126.com

depositional age was between the late Neoproterozoic and the early Cambrian. (3) Lai et al. (2014) applied the software G-Plate along with igneous rock ages to reconstruct the tectonic development of Southeast Asia and proposed a new tectonic model for SW South China–Eastern Indochina. In this model, the ALS Group formed during the Silurian-Devonian. These apparent discrepancies in depositional age may not only result from the complicated tectonic environment of the ALS-RR shear zone, but also from the lack of adequate, accurate and directed geochronological data from the high-grade metamorphic sedimentary successions of the ALS Group. Systematic geochemical analysis and pinpointed zircon U-Pb dating of the metasedimentary rocks of the ALS Group will shad lights to the debate.

In this study, we first briefly introduce the geological setting of ALS metamorphic belt and then present a set of new whole-rock geochemical data and in-situ zircon U-Pb ages of both the inherited cores and the overgrowth rims of rocks with different metamorphic grades in the ALS Group. Our geochemical and geochronological investigations concentrated on the clastic rocks of the ALS Group to preliminarily identify their provenance, depositional environment and age.

2 Geological Setting

The ALS belt in the southeastern Tibetan Plateau is separated from the SCB by the Red River fault in the east and from the Indochina Block by the Anding-Jiujia fault in the west, and this NW-SE-trending belt is over 500 km long and 10 to 50 km wide (BGMRY, 1990; Deng et al., 2014; Liu et al., 2015; Faure et al., 2016; Fig. 1a). Between the two bounding faults, the ALS fault divides the ALS belt into two distinct metamorphic units (Fig. 1b). The high-grade metamorphic unit in the east, the main focus in this paper, experienced low amphibolite-facies to granulite-facies metamorphism (Liu F L et al., 2013; Liu J L et al., 2015; Wang et al., 2016; Liu et al., 2017), although the metamorphic grade locally (adjacent to the ALS fault) reaches greenschist facies. In this unit, a set of NW-SE-striking Cenozoic strike-slip or high-angle reverse faults divide the belt into elongated and narrow strips (Faure et al., 2016). Although the metasedimentary rocks of the ALS Group have been (unsuitably) subdivided into four formations from southwest to northeast in previous works, i.e. Xiaoyangjie, Along, Fenggang and Wudukeng formations (BGMRY, 1990; Fig. 2), these formations are often in contact with faults or shear zones and lack distinct or continuous stratigraphy (Liu J L et al., 2015). Consequently, these units do not reflect actual sedimentary sequence relations. The only differences among the formations are based on lithologic discrepancies. Among these units, the Xiaoyangjie Formation consists predominantly of two-mica schist, psammite, and quartzite, whereas the Along Formation is mainly

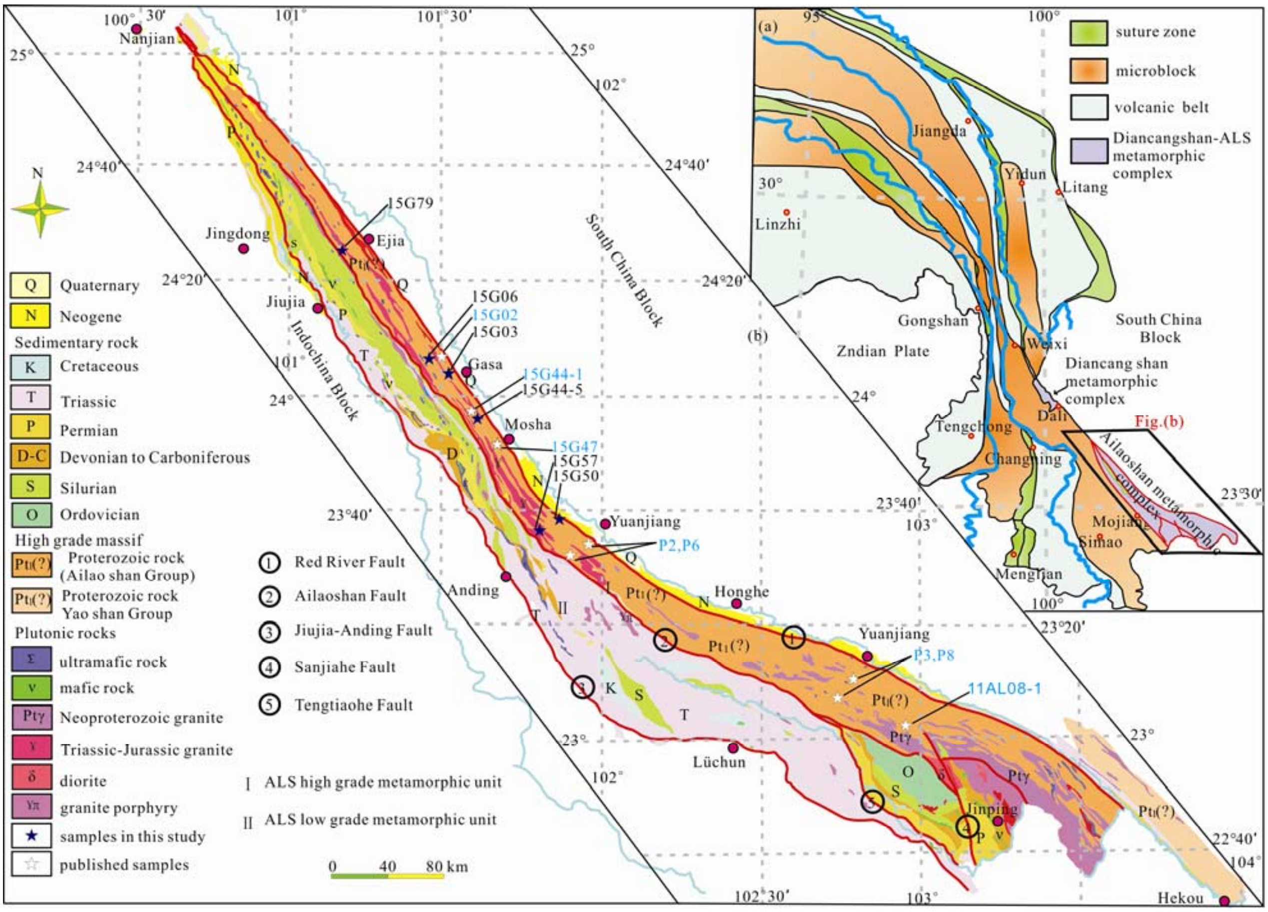

Fig. 1. Tectonic sketch map of Sanjiang tectonic zone and Ailaoshan metamorphic complex, southwestern China.
(a) Simplified tectonic subdivision of the Sanjiang area, southeastern Tibetan Plateau (modified after Deng jun et al., 2014); (b) geological map of the Ailaoshan metamorphic complex, showing the locations of the dated samples (modified after Liu junlai et al., 2015).

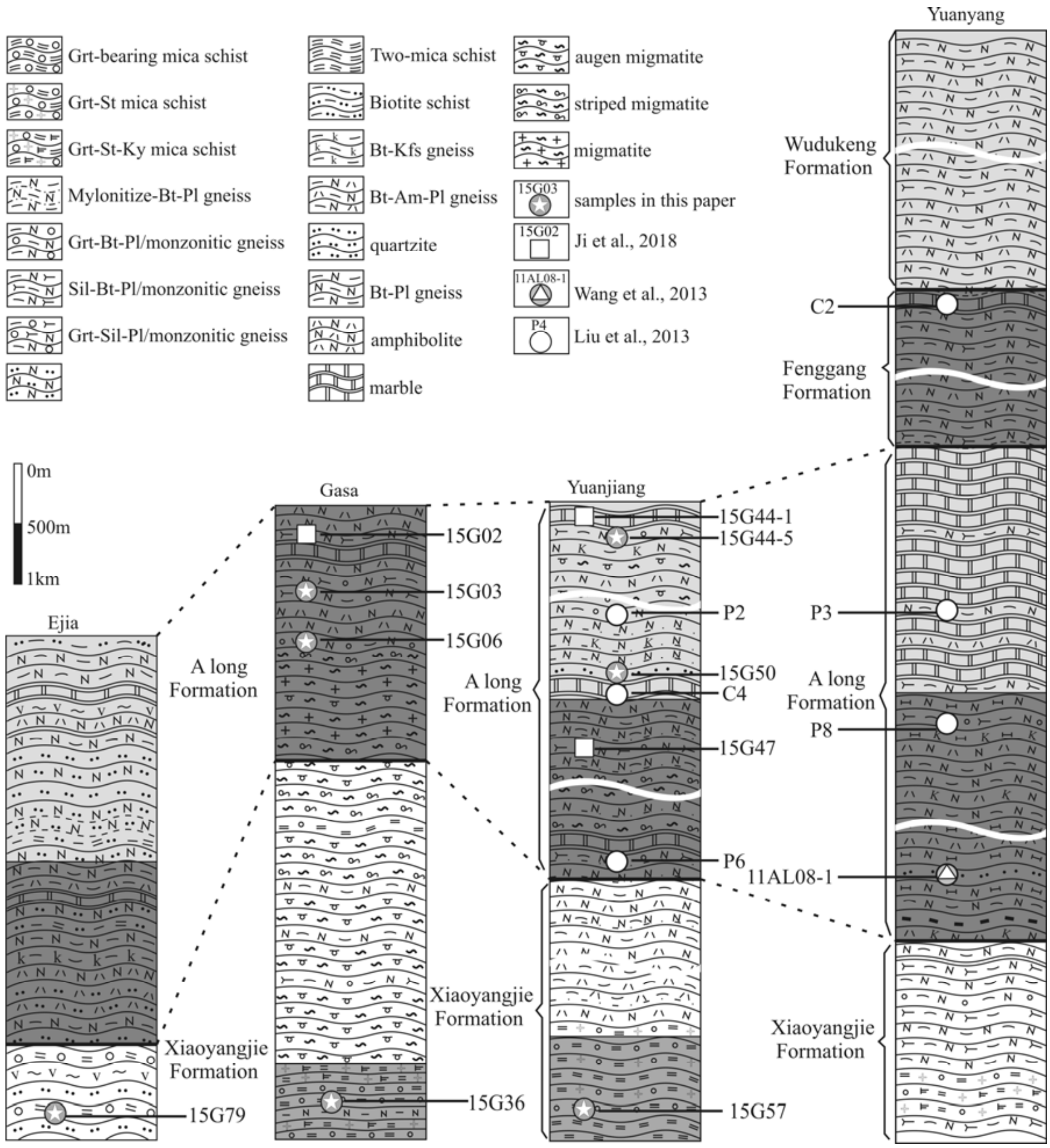

Fig. 2. Stratigraphic columns for the Ailaoshan Group (modified from the 1:200,000 geological maps of Weishan, Xinping, Mojiang, Yuanyang and Jingping, Yunnan).
The star symbols denote the locations of the collected samples. The stratigraphic columns show wavy patterns reflecting a metamorphic history.

composed of marble, calcsilicate, metapelite (garnet-sillimanite-biotite gneiss and kyanite-bearing garnet-sillimanite-biotite gneiss), and amphibolites containing thin layers of metapelite and fine-grained metasandstones (YGS, 1975, 1976a, 1976b). The distributions of the Fenggang and Wudukeng formations are limited to the southern segment of the ALS belt (YGS, 1976c). The Wudukeng Formation is lithologically similar to the Along Formation and makes up two limbs of an isoclinal fold inclined to the northeast (BGMRY, 1990). In the southern segment of the ALS belt, intense left-lateral shearing occurred in the Oligocene, and most rocks in the high-grade metamorphic units exhibit extremely narrow and long mylonite zones. Additionally, magmatic activity occurred in the Neoproterozoic, Indonesian, and Oligocene. Neoproterozoic acidic and mafic plutons dominate the southern segment of the ALS belt (Yuanjiang-Jinping area, Qi et al., 2012, 2014, 2016; Cai et al., 2014, 2015; Wang et al., 2016; Chen et al., 2017) and may be associated with the Panxi-Hannan belt, which is related to a long-lived Neoproterozoic (900-720 Ma) subduction zone in the southwestern and northwestern margins of the Yangtze Block (Wang et al., 2016; Chen et al., 2017). The Indonesian and Cenozoic magmatic rocks in the ALS belt are widespread and comprise multiple types, such as subduction-related granitoids and rhyolites and anatectic S-type granite resulting from terrane collision orogenesis (Zi et al., 2012; Liu et al., 2014; Wang et al., 2017; Wu et al., 2017) and the syn- and post-kinematic effects of crustal-scale shearing during the Cenozoic (Liu J L et al., 2015).

To the west of the high-grade unit, bounded by the ALS fault and the Anding-Jiujia fault, Silurian-Permian volcano-sedimentary strata and marine sedimentary rocks (BGMRY, 1990; Wang et al., 2014) are predominantly unmetamorphosed or are greenschist-facies (Liu F L et al., 2015; Wang et al., 2016) slates, phyllites, greenschists, quartzites, and carbonates (Fan et al., 2010; Wang et al., 2014). These Phanerozoic strata are recognized as sediments of the Jinsha Jiang-ALS-Song Ma Ocean (northern branch of the Palaeo-Tethys Ocean). The Indosinian orogeny is marked by a regional unconformity between Permian and Triassic strata (Wang et al., 2014; Xia et al., 2016). In this low-grade metamorphic unit (northeastern Indochina Block), intensive and extensive magmatism occurred during the Permo-Triassic (280–210 Ma), which was related to Palaeo-Tethys oceanic subduction, closure and syn- or post-collision processes between the Indochina Block and the SCB (Liu F L et al., 2013; Lai et al., 2014; Wang et al., 2017; Wu et al., 2017)

3 Samples and Analytical Methods

3.1 Sample description

Eleven metasedimentary samples were collected from the ALS Group for whole-rock geochemical analysis, and zircons were separated from 6 of them, including two-mica schists (15G57, 15G79), greywacke (15G50-1), garnet-sillimanite-biotite gneisses (15G03, 15G06) and kyanite-bearing garnet-sillimanite-biotite gneiss (15G44). The approximate locations of the zircon samples are marked in Fig. 1b. Specifically, samples 15G57 and 15G79 were collected from the Xiaoyangjie Formation, while samples 15G57 and 15G79 were collected from the Along Formation (Fig. 2). The specific location, lithologies, mineral components and metamorphic grade of each sample in this paper, as well as previously published results, are described in Table 1. The photomicrographs in Fig. 3a-d show the mineral occurrence form and microstructure.

3.2 Analytical techniques

3.2.1 Geochemical

For the whole-rock analyses, samples were crushed to 200-mesh using an agate mill. The abundances of major elements were determined at the National Research Center of Geoanalysis, Beijing, China, by X-ray fluorescence spectrometry (3080E). In addition, rare earth element (REE) and other trace element concentrations were determined by inductively coupled plasma mass spectrometry (ICP-MS).

3.2.2 Zircon U-Pb geochronology

Transmitted and reflected light photomicrographs were first processed to avoid fractures and inclusions in the zircon grains. To observe the inner structural features of zircon, cathodoluminescence (CL) imaging was conducted with an FEI 450 scanning electron microscope with an attached Gatan CL4 system. The LA-ICP-MS zircon U–Pb analyses were carried out at the Analysis Centre in the Shandong Bureau of China Metallurgical Geology Bureau using a Thermo Xseries2 ICP-MS instrument equipped with a Geolas Pro 193 nm laser ablation system. The diameter of the laser ablation craters was 25 μm. The $^{207}Pb/^{206}Pb$, $^{206}Pb/^{238}U$ and $^{207}Pb/^{235}U$ ratios were calculated using the software ICPMSDateCal and were then corrected using GJ-1 (Jackson et al., 2004) as an external calibrant. The Harvard zircon 91500, with a $^{207}Pb/^{206}Pb$ age of 1065.4±0.6 Ma and a $^{206}Pb/^{238}U$ age of 1062.4±0.8 Ma (Wiedenbeck et al., 1995), was used as an external standard to normalize the isotopic discrimination. NIST610 glass was used as an external standard to normalize the U, Th, and Pb concentrations of the unknowns. The isotopic data were processed using the program Isoplot/Ex (version 3.0) (Ludwig, 2003). The detailed operational conditions of the laser ablation system and the ICP-MS instrument and the data reduction process are the same as those described by Liu et al. (2008).

4 Results

A total of 11 samples from the different parts of the ALS Group were selected for major and trace element analysis, and more than one analysis was conducted on two samples (15G44 and 15G47). The major and trace element data are listed in Table 2. The degree of weathering of these samples is first identified and shown in Fig. 4a–b. The minor elements and REEs are normalized to the upper continental crust (UCC) and chondrites, and the results are shown in Fig. 4c–d, respectively.

The U-Pb isotope results of detrital zircon grains from six metasedimentary rocks in the ALS Group are presented in Table 3. The CL images showing the inner

Table 1 Summary of zircon LA-ICP-MS U-Pb analysis samples reported in this study and from previous work, including sample name, location, lithology and mineral assemblage.

Sample name	Latitude	Longitude	Location	Lithology	Mineral assemblage	Formation	Reference
15G50	23°46′22″	101°44′27″	Mosha	Quartzite	Qtz+Pl	Along	This study
15G79	24°25′45″	101°10′27″	Ejia	Mica-schist	Mu+Bt+Qtz+Pl+Grt	Xiaoyangjie	This study
15G57	23°46′05″	101°42′31″	Mosha	Mica-schist	Mu+Bt+Qtz+Pl+Grt	Xiaoyangjie	This study
15G03	24°05′51″	101°30′45″	Gasa	Metapelite	Grt+Sil+Qtz+Pl+Kfs	Along	This study
15G06	24°05′08″	101°31′30″	Gasa	Metapelite	Grt+Sil+Qtz+Pl+Kfs	Along	This study
15G44-5	23°55′56″	101°38′35″	Yaojie	Metapelite	Grt+Sil+Qtz+Pl+Kfs+Ky	Along	This study
15G02	24°06′00″	101°30′35″	Gasa	Metapelite	Grt+Sil+Qtz+Pl+Kfs	Along	Ji et al., 2018
15G44-1	23°55′55″	101°38′33″	Yaojie	Domatic mable	Dol+Cal+Phl+	Along	Ji et al., 2018
15G47	23°50′00″	101°42′13″	Yaojie	Metapelite	Grt+Sil+Qtz+Pl+Kfs	Along	Ji et al., 2018
11AL08-1	23°04′40″	102°59′20″	Yuanyang	Quartzite	Qtz (>95%) +Ms+Pl+Am	Along	Wang et al., 2013

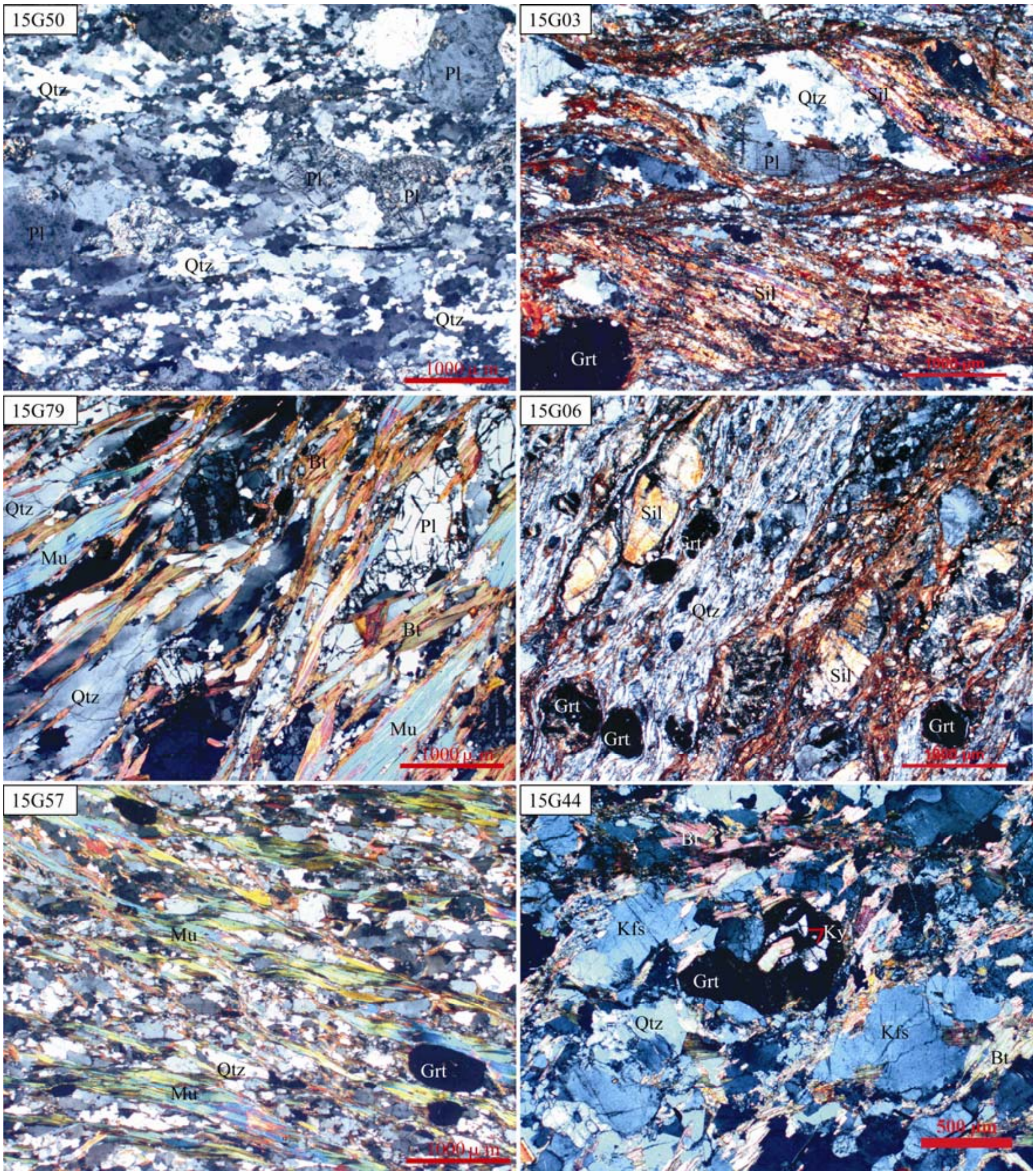

Fig. 3. Photomicrographs of samples from the metasedimentary rocks in the Ailaoshan Group. (All images are under cross-polarized light.)
Abbreviations for minerals: Qtz, quartz; Pl, plagioclase; Kfs, K-feldspar; Bt, biotite; Mu, muscovite; Grt, garnet; Sil, sillimanite.

structures of the zircons are shown in Fig. 5. Concordia plots for all analysed zircons and a relative probability density diagram of detrital zircon ages are presented in Fig. 6 and Fig. 7, respectively.

4.1 Geochemistry

The metapelite from the ALS Group shows notable variation in SiO_2 content (from 61.21 to 74.79 wt%), and the TiO_2 content (0.69–1.21 wt%) is high owing to intense chemical weathering, resulting in chemical index of alternation (CIA) values ranging from 60 to 73. In contrast, the quartzite from the ALS Group has relatively low Al_2O_3 (6.97–6.65 wt%), $Fe_2O_3^T$ (0.06–0.53 wt%) and MgO (0.03–0.16 wt%) contents but distinctly higher SiO_2 content (87.76–86.93 wt%), corresponding to lower CIA values (54 and 55). The mica-quartz schist from the Xiaoyangjie Formation exhibits limited ranges of SiO_2 (64.69–70.22 wt%) and Al_2O_3 (14.18–15.82 wt%) and moderate $Fe_2O_3^T$ (4.64–5.90 wt%) and MgO (1.79–2.54 wt%) contents. The relatively high H_2O^+ values (1.03–2.6 wt%) reflect high concentrations of muscovite. The two greywacke samples have the highest relative Na_2O+K_2O contents (ca. 8%) but the lowest CIA values (52–53). The variation in the CaO contents among the analysed samples

Table 2 Whole-rock major and trace element results for metasedimentary rocks from the Ailaoshan Group

Sample	15G50-1	15G74-1	15G57	15G79	15G36	15G30-1	15G60-1	15G03	15G06	15G44-5	15G44-6	15G47-1	15G47-6
	Quartzite		Schist			Greywacke		Metapelite					
Major element (wt%)													
SiO_2	87.76	86.93	70.22	68.32	64.69	72.48	62.9	66.41	74.79	61.3	61.21	70.48	68.51
TiO_2	0.25	0.07	0.62	0.69	0.67	0.48	0.46	0.82	0.69	1.24	0.99	0.75	0.77
Al_2O_3	6.65	6.97	14.18	15.24	15.82	11.96	17.37	16.15	12.31	17.78	17.34	15.39	15.79
FeO	0.34	0.05	3.72	2.93	4.44	1.38	4.01	3.83	3.65	3.22	6.92	3.68	3.43
Fe_2O_3	0.19	0.01	0.92	2.09	1.46	2.89	0.2	0.76	0.62	2.41	1.68	1.03	1.51
MnO	0.02	0.01	0.1	0.05	0.11	0.13	0.09	0.07	0.07	0.05	0.13	0.07	0.06
MgO	0.16	0.03	1.79	1.93	2.54	0.31	2.46	1.84	1.47	2.54	2.44	1.63	1.61
CaO	0.41	0.18	1.68	0.81	1.66	1.2	2.76	1.48	1.26	1.85	1.43	0.66	0.72
Na_2O	1.13	0.72	2.88	0.68	2.4	2.65	4.01	2.2	1.18	2.11	1.08	0.73	0.85
K_2O	2.62	4.34	2.38	3.31	3.5	5.38	4	4.73	2.75	4.41	3.92	3.55	3.69
P_2O_5	0.04	0.02	0.12	0.15	0.13	0.04	0.14	0.11	0.09	0.32	0.17	0.12	0.12
H_2O^+	0.32	0.24	1.03	2.6	1.6	0.49	1.01	0.98	0.73	1.66	1.77	0.99	1.94
CO_2	0	0.09	0.34	0.26	0.34	0.51	0.34	0.26	0.34	0.51	0.6	0.09	0.43
Total	99.89	99.66	99.98	99.06	99.36	99.9	99.75	99.64	99.95	99.40	99.68	99.17	99.43
CIA	55	54	60	73	61	52	53	60	66	63	71	72	73
ICV	0.95	0.92	1.15	0.87	1.20	1.30	1.32	1.09	0.99	1.19	0.99	0.78	0.81
Trace elements (ppm)													
La	18.3	20.9	24.5	54.4	38.0	132.0	33.1	59.9	50.1	125.0	102.0	57.7	71.0
Ce	35.7	39.5	49.9	105	75.4	287.0	66.1	117.0	96.7	269.0	203.0	110.0	127.0
Pr	4.02	4.24	6.15	12.2	9.0	29.8	7.46	13.2	10.9	28.9	20.9	12.5	14.7
Nd	14.6	16	23.7	49	37.1	105.0	28.3	50.9	41.9	105.0	74.2	49.8	55.8
Sm	2.33	2.83	4.83	8.67	7.34	17.9	5.01	9.2	7.16	18.9	13.4	8.68	9.65
Eu	0.67	0.85	1.06	1.54	1.14	1.99	1.03	1.69	1.35	2.2	1.47	1.23	1.16
Gd	1.95	1.88	4.33	7.42	6.91	15.7	3.97	7.35	5.78	14.4	11.7	7.54	8.36
Tb	0.26	0.28	0.76	1.27	1.25	2.72	0.65	1.16	0.94	1.76	1.86	1.16	1.23
Dy	1.43	1.42	4.54	6.87	7.30	15.30	3.59	6.63	5.44	6.69	10.80	6.66	6.64
Ho	0.29	0.27	0.92	1.3	1.42	2.96	0.68	1.29	1.05	0.95	2.1	1.3	1.21
Er	0.83	0.7	2.84	3.74	4.32	9.1	2.05	3.7	3.12	2.62	6.23	3.86	3.43
Tm	0.13	0.11	0.42	0.5	0.64	1.29	0.28	0.56	0.46	0.34	0.97	0.56	0.5
Yb	0.8	0.59	2.59	2.96	4.06	8.3	1.82	3.63	2.95	2.19	6.09	3.47	3.12
Lu	0.13	0.08	0.41	0.44	0.58	1.21	0.29	0.53	0.43	0.35	0.91	0.52	0.47
Sc	2.91	2	12.4	14.9	15	4.88	12.6	12.9	10.8	8.69	18.8	12.7	12.4
V	12.9	5.43	71.3	95.2	78.2	2.3	73.4	84.0	63.9	119.0	110.0	75.4	83.4
Cr	12.8	6.69	51.8	85.2	84.1	0.5	28.7	82.2	57.2	118.0	209.0	70.8	90.0
Co	1.99	0.35	12.4	16.2	15.0	0.4	11.6	11.7	10.7	18.5	15.9	8.1	8.0
Ni	2.81	0.58	24	34.2	36.8	0.6	14.9	24.3	25.3	37.5	39.7	14.6	22.1
Cu	4.1	1.71	8.3	16.8	58.9	1.6	8.68	13.0	31.5	40.5	48.2	12.7	23.0
Rb	93	158	154	186	239	116	247	160	93	200	164	160	160
Sr	71.4	54	143	60.2	100	71.6	183	88.9	117	140	96.2	101	109
Y	7.54	6.18	23.5	33.3	37.4	77.4	17	34	29	25	55.7	34.9	30.9
Zr	222	47.7	164	252	217	1095	135	386	369	570	531	294	320
Nb	6.56	1.54	12.3	12.9	14	117	10.4	13.9	12.7	20.7	19.9	15.3	15.6
Ba	655	3027	399	537	457	149	829	936	544	750	956	750	660
Hf	6.33	1.66	5.26	8.05	6.48	23.8	4.53	11	9.67	14.1	12.7	8.8	9.64
Th	8.49	2.66	7.8	22.6	14.9	19.5	17.8	24.8	20.8	49.2	49.7	24	36.8
U	0.97	0.84	3.01	4.86	4.84	3.28	6.54	4.16	2.81	6.64	3.88	5.23	5.27
Zn	7.25	2.73	71.1	79.5	98.0	152.0	76.2	78.1	37.9	111.0	92.5	82.2	91.9
Pb	17	25.3	22.6	27.8	16.4	14.1	34.1	15.9	7.7	18.0	12.6	26.0	26.0
Ta	0.5	0.22	1.42	1.16	1.04	7.29	1.38	0.85	0.8	1.1	1.18	1.24	1.03
Ga	7.93	6.73	18.4	18.7	18.2	27.9	20.2	22.1	14.7	26.0	24.1	22.9	23.8
Cs	1.47	7.21	14.6	16.1	27.0	1.2	21.8	4.0	1.3	3.7	11.3	5.3	5.3
ΣREE	81	90	127	255	194	630	154	277	228	578	456	265	304
$(La/Yb)_N$	22.9	35.4	9.5	18.4	9.4	15.9	18.2	16.5	17.0	57.1	16.7	16.6	22.8
Eu/Eu*	0.31	0.36	0.23	0.19	0.16	0.12	0.23	0.20	0.21	0.13	0.12	0.15	0.13
Zr/Hf	35.07	28.73	31.18	31.30	33.49	46.01	29.80	35.09	38.16	40.43	41.81	33.41	33.20
Rb/Sr	1.30	2.93	1.08	3.09	2.39	1.62	1.35	1.80	0.79	1.43	1.70	1.58	1.47
Th/U	8.75	3.17	2.59	4.65	3.08	5.95	2.72	5.96	7.40	7.41	12.81	4.59	6.98
Zr/Sc	76.29	23.85	13.23	16.91	14.47	224.39	10.71	29.92	34.17	65.59	28.24	23.15	25.81
La/Sc	6.29	10.45	1.98	3.65	2.53	27.05	2.63	4.64	4.64	14.38	5.43	4.54	5.73
Th/Sc	2.92	1.33	0.63	1.52	0.99	4.00	1.41	1.92	1.93	5.66	2.64	1.89	2.97

Note: CIA = $[Al_2O_3/(Al_2O_3 + CaO^* + Na_2O + K_2O)] \times 100$ where CaO* represents Ca in silicate-bearing minerals only and all in molecular proportions; ICV = $(Fe_2O_3 + K_2O + Na_2O + CaO + MgO + TiO_2)/Al_2O_3$

is not significant. In the A-C+N-K ternary diagram (Fig. 4a, Nesbitt and Young, 1982, 1989; Fedo et al., 1995), most samples plotted roughly along the predicted weathering trend, except for one quartzite sample (15G74) exhibiting slight potassium (K) metasomatism, which was excluded from the U-Pb dating process. In the diagram of CIA vs. the index of compositional variability (ICV) (Fig. 4b, Nesbitt and Young, 1984; Cox et al., 1995), all samples plot within the weak to moderate weathering field.

In terms of trace element data, the quartzite and

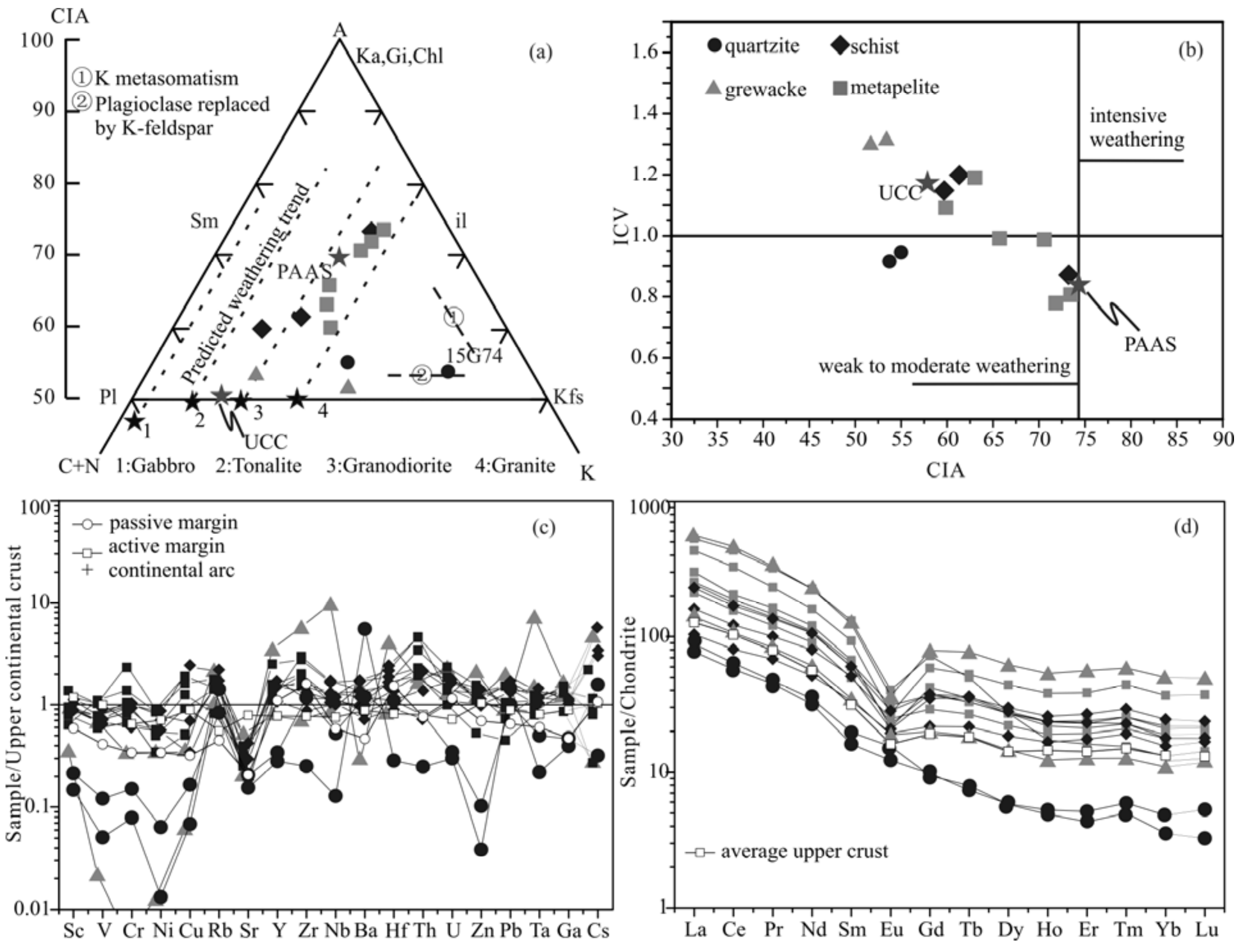

Fig. 4. Major and minor elements geochemical diagrams of metasedimentary rocks from ALS Group.
(a) A-CN-K ternary diagram (in molecular proportions) (after Nesbitt and Young, 1982; Fedo et al., 1995). The possible post-depositional alteration is represented by trend 1 (K metasomatism) and trend 2 (replacement of plagioclase by K-feldspar). Mineral abbreviations: ka = kaolinite, gi = gibbsite, chl = chlorite, sm = smectite, il = illite, kfs = potassium feldspar, plag = plagioclase, An = anorthite, Ab = albite. (b) CIA vs. ICV diagram (after Nesbitt and Young, 1984; Cox et al., 1995) to show the maturity and degree of chemical weathering of the studied rocks. (c) Normalized to average upper continental crustal values (after Floyd et al., 1991). (d) REEs normalized to chondrites (after Taylor and McLennan, 1985).

greywacke samples have significantly low transitional element contents, such as Sc, V, Cr, Co and Ni, whereas the metapelite and garnet-bearing mica-quartz schist have relatively high transitional element contents. The Rb and Ba contents range from 93 to 247 ppm and from 149 to 3027, respectively. In addition, the concentrations of Sr in all of the analysed samples are lower than the UCC value (350 ppm, Talor and McLennan, 1985) and vary between 54 ppm and 183 ppm. In the average UCC-normalized trace element diagrams (Fig. 4c), the rocks exhibit positive Zr, Th, Hf, Nb and Y anomalies and negative Sr, V, Cr and Ni anomalies.

In the chondrite-normalized REE diagram (Fig. 4d), the REE patterns of the metasedimentary rocks are similar to that of the UCC. The quartzite samples have low ΣREE contents (81–90 ppm), which are significantly lower than the UCC value (Talor and McLennan, 1985). The ΣREE concentrations of metapelite and garnet-bearing mica-quartz schist range from 228 ppm to 578 ppm. The differences between the quartzite and the other metasedimentary rocks is the lack of negative Eu anomalies, Eu/Eu^* values ranging from 0.31 to 0.36 and high La/Yb_N values (22.9–35.4).

4.2 U-Pb dating

In total, six hundred and ninety-five detrital zircon U-Pb analytical data points are listed in Table 3. More than 110 analyses, including spots in concentric oscillatory cores and overgrowth rims, were conducted on zircon grains from each sample to avoid information loss on the source area based on statistical principles (Fedo et al., 2003). For the greywacke (15G50) and two-mica schist (15G79 and 15G57), U-Pb chronological data with discordances >10% and large uncertainties (>100 Ma at 1σ uncertainty) were excluded from consideration. For the Al-rich gneiss samples (15G03, 15G06, 15G44), data with discordances >15% and large uncertainties (>30 Ma at 1σ uncertainty for ages <1000 Ma) were excluded, and the measured $^{207}Pb/^{206}Pb$ ages were used when the $^{206}Pb/^{238}U$ ages were older than 1000 Ma. All dates were handled by the Isoplot 3.0 application package.

4.2.1 Sample 15G50

The zircon grains from sample 15G50 are 150–250 mm

Table 3 LA-ICP-MS dating of detrital zircons from metasedimentary rocks in the ALS Group, southwestern South China Block

Grain No.	Element (ppm)		Th/U	$^{207}Pb/^{235}U$	1σ	$^{206}Pb/^{238}U$	1σ	Age (Ma)						Concor	Used ages		Postion
	Th	U						$^{207}Pb/^{206}Pb$	1σ	$^{207}Pb/^{235}U$	1σ	$^{206}Pb/^{238}U$	1σ				
15G50, Greywacke																	
15G50-26	84	386	0.22	0.5574	0.0142	0.0707	0.0011	498	48	450	9	440	6	97%	440	6	Core
15G50-84	54	234	0.23	0.5742	0.0346	0.0707	0.0038	567	60	461	22	441	23	95%	441	23	Core
15G50-52	113	129	0.87	0.5859	0.0210	0.0738	0.0017	502	71	468	13	459	10	97%	459	10	Core
15G50-51	75	40	1.86	0.5876	0.0321	0.0745	0.0015	502	130	469	21	463	9	98%	463	9	Core
15G50-07	98	402	0.24	0.6234	0.0200	0.0746	0.0018	617	86	492	13	464	11	94%	464	11	Rim
15G50-60	88	70	1.25	0.5872	0.0220	0.0747	0.0012	498	87	469	14	464	7	98%	464	7	Core
15G50-101	60	199	0.30	0.6417	0.0237	0.0771	0.0017	620	71	503	15	479	10	95%	479	10	Core
15G50-92	246	224	1.10	0.5908	0.0163	0.0772	0.0012	432	62	471	10	480	7	98%	480	7	Core
15G50-61	175	75	2.34	0.6345	0.0254	0.0773	0.0014	591	87	499	16	480	8	96%	480	8	Core
15G50-22	26	484	0.05	0.6513	0.0211	0.0776	0.0011	632	63	509	13	482	6	94%	482	6	Rim
15G50-36	116	79	1.47	0.6029	0.0209	0.0784	0.0015	456	70	479	13	487	9	98%	487	9	Core
15G50-83	199	99	2.01	0.6186	0.0217	0.0786	0.0012	502	69	489	14	488	7	99%	488	7	Core
15G50-50	462	201	2.30	0.6673	0.0227	0.0793	0.0019	620	58	519	14	492	12	94%	492	12	Core
15G50-40	180	321	0.56	0.6684	0.0190	0.0819	0.0014	572	58	520	12	507	8	97%	507	8	Core
15G50-39	353	271	1.30	0.6555	0.0187	0.0820	0.0012	524	56	512	11	508	7	99%	508	7	Core
15G50-78	71	70	1.00	0.6905	0.0229	0.0845	0.0015	572	63	533	14	523	9	98%	523	9	Core
15G50-87	55	70	0.79	0.6930	0.0340	0.0847	0.0012	569	90	535	20	524	7	98%	524	7	Core
15G50-90	31	47	0.65	0.6963	0.0303	0.0851	0.0016	569	84	537	18	527	9	98%	527	9	Core
15G50-27	72	269	0.27	0.7133	0.0211	0.0881	0.0013	567	56	547	13	544	8	99%	544	8	Core
15G50-103	58	130	0.45	0.7336	0.0298	0.0892	0.0021	591	71	559	17	551	12	98%	551	12	Core
15G50-113	116	259	0.45	0.7412	0.0182	0.0901	0.0017	598	48	563	11	556	10	98%	556	10	Core
15G50-44	37	75	0.50	0.7526	0.0292	0.0905	0.0023	613	72	570	17	558	14	97%	558	14	Core
15G50-45	73	148	0.50	0.7427	0.0235	0.0907	0.0016	576	66	564	14	560	10	99%	560	10	Core
15G50-37	40	60	0.66	0.7780	0.0290	0.0913	0.0015	665	77	584	17	564	9	96%	564	9	Core
15G50-79	150	190	0.79	0.7536	0.0203	0.0920	0.0016	583	52	570	12	567	9	99%	567	9	Core
15G50-67	55	157	0.35	0.7627	0.0199	0.0933	0.0013	589	54	576	11	575	8	99%	575	8	Core
15G50-82	109	54	2.03	0.7490	0.0241	0.0935	0.0015	543	68	568	14	576	9	98%	576	9	Core
15G50-95	210	119	1.76	0.7893	0.0272	0.0948	0.0018	633	73	591	15	584	11	98%	584	11	Core
15G50-66	9	30	0.30	0.7890	0.0434	0.0960	0.0021	583	115	591	25	591	12	99%	591	12	Core
15G50-33	30	67	0.45	0.8017	0.0267	0.0976	0.0017	583	59	598	15	600	10	99%	600	10	Core
15G50-20	39	62	0.63	0.7888	0.0396	0.0979	0.0022	539	95	590	23	602	13	98%	602	13	Rim
15G50-116	56	146	0.39	0.8263	0.0245	0.0986	0.0019	628	52	612	14	606	11	99%	606	11	Core
15G50-69	162	96	1.69	0.8137	0.0290	0.0993	0.0017	589	73	605	16	611	10	99%	611	10	Core
15G50-31	46	56	0.82	0.8302	0.0290	0.1002	0.0018	613	69	614	16	616	11	99%	616	11	Core
15G50-53	45	121	0.37	0.8642	0.0269	0.1026	0.0016	633	73	632	15	629	10	99%	629	10	Core
15G50-64	9	23	0.40	0.8846	0.0435	0.1042	0.0029	680	106	643	23	639	17	99%	639	17	Core
15G50-46	70	98	0.72	0.9893	0.0334	0.1044	0.0024	876	47	698	17	640	14	91%	640	14	Core
15G50-80	49	98	0.50	0.8874	0.0307	0.1045	0.0022	661	61	645	17	641	13	99%	641	13	Core
15G50-49	45	299	0.15	0.9690	0.0407	0.1057	0.0034	798	52	688	21	648	20	94%	648	20	Core
15G50-62	47	215	0.22	0.9397	0.0259	0.1071	0.0016	720	48	673	14	656	9	97%	656	9	Core
15G50-65	25	90	0.28	0.9665	0.0322	0.1093	0.0019	746	65	687	17	669	11	97%	669	11	Core
15G50-10	78	188	0.42	1.0006	0.0312	0.1108	0.0023	783	61	704	16	677	13	96%	677	13	Rim
15G50-59	112	512	0.22	1.0707	0.0237	0.1110	0.0012	917	43	739	12	678	7	91%	678	7	Core
15G50-81	26	60	0.44	0.9657	0.0346	0.1126	0.0021	683	69	686	18	688	12	99%	688	12	Core
15G50-71	74	85	0.88	0.9712	0.0339	0.1128	0.0019	687	67	689	17	689	11	99%	689	11	Core
15G50-99	21	49	0.42	0.9874	0.0402	0.1147	0.0022	700	83	697	21	700	12	99%	700	12	Core
15G50-15	72	445	0.16	1.0528	0.0227	0.1159	0.0014	796	45	730	11	707	8	96%	707	8	Rim
15G50-86	33	80	0.41	0.9957	0.0302	0.1161	0.0020	687	58	702	15	708	11	99%	708	11	Core
15G50-43	188	269	0.70	1.1660	0.0429	0.1228	0.0035	883	48	785	20	747	20	95%	747	20	Core
15G50-72	34	67	0.51	1.1114	0.0355	0.1250	0.0024	763	68	759	17	759	14	99%	759	14	Core
15G50-112	39	68	0.57	1.1164	0.0332	0.1252	0.0020	769	61	761	16	760	11	99%	760	11	Core
15G50-47	59	39	1.51	1.1772	0.0513	0.1253	0.0019	865	89	790	24	761	11	96%	761	11	Core
15G50-91	91	88	1.03	1.2596	0.0405	0.1357	0.0026	856	54	828	18	820	15	99%	820	15	Core
15G50-35	87	522	0.17	1.3125	0.0297	0.1384	0.0024	900	31	851	13	836	14	98%	836	14	Core
15G50-106	95	323	0.29	1.3168	0.0358	0.1405	0.0025	866	44	853	16	848	14	99%	848	14	Core
15G50-09	192	387	0.50	1.4272	0.0403	0.1432	0.0036	987	46	900	17	863	20	95%	863	20	Rim
15G50-28	218	212	1.03	1.3782	0.0302	0.1440	0.0019	910	37	880	13	867	11	98%	867	11	Core
15G50-18	64	817	0.08	1.3892	0.0412	0.1442	0.0029	915	42	884	18	869	16	98%	869	16	Rim
15G50-97	77	168	0.46	1.3773	0.0425	0.1452	0.0026	887	81	879	18	874	14	99%	874	14	Core
15G50-98	183	447	0.41	1.4205	0.0338	0.1484	0.0019	911	44	898	14	892	10	99%	892	10	Core
15G50-29	111	275	0.40	1.4414	0.0337	0.1485	0.0025	943	42	906	14	892	14	98%	892	14	Core
15G50-41	40	52	0.77	1.4266	0.0498	0.1494	0.0026	900	67	900	21	898	15	99%	898	15	Core
15G50-89	153	246	0.62	1.4485	0.0326	0.1501	0.0025	931	34	909	14	902	14	99%	902	14	Core
15G50-68	30	28	1.06	1.4528	0.0511	0.1502	0.0022	931	69	911	21	902	12	99%	902	12	Core
15G50-38	155	131	1.18	1.4411	0.0310	0.1502	0.0024	917	45	906	13	902	14	99%	902	14	Core
15G50-108	17	27	0.64	1.5092	0.0522	0.1572	0.0028	924	67	934	21	941	16	99%	941	16	Core
15G50-76	352	371	0.95	1.5272	0.0346	0.1579	0.0025	931	38	941	14	945	14	99%	945	14	Core
15G50-48	109	204	0.53	1.6360	0.0366	0.1586	0.0026	1054	43	984	14	949	14	96%	949	14	Core
15G50-75	63	172	0.37	1.5618	0.0410	0.1586	0.0030	969	41	955	16	949	17	99%	949	17	Core
15G50-107	59	171	0.34	1.5833	0.0417	0.1602	0.0018	976	54	964	16	958	10	99%	958	10	Core

Continued Table 3

Grain No.	Element (ppm)		Th/U					Age (Ma)						Concor	Used ages		Postion
	Th	U		$^{207}Pb/^{235}U$	1σ	$^{206}Pb/^{238}U$	1σ	$^{207}Pb/^{206}Pb$	1σ	$^{207}Pb/^{235}U$	1σ	$^{206}Pb/^{238}U$	1σ				
15G50-111	48	105	0.45	1.5716	0.0434	0.1606	0.0029	967	48	959	17	960	16	99%	960	16	Core
15G50-73	47	86	0.55	1.5806	0.0517	0.1615	0.0027	950	56	963	20	965	15	99%	965	15	Core
15G50-88	91	162	0.56	1.5725	0.0411	0.1616	0.0026	946	48	959	16	966	14	99%	966	14	Core
15G50-34	95	58	1.62	1.6701	0.0595	0.1641	0.0033	1031	64	997	23	980	18	98%	980	18	Core
15G50-74	14	37	0.39	1.7682	0.0813	0.1686	0.0033	1100	89	1034	30	1004	18	97%	1100	89	Core
15G50-56	18	81	0.23	1.7792	0.0507	0.1693	0.0030	1094	57	1038	19	1008	17	97%	1094	57	Core
15G50-63	55	269	0.20	1.7133	0.0428	0.1701	0.0030	1015	44	1014	16	1013	17	99%	1015	44	Core
15G50-109	184	455	0.40	1.7674	0.0446	0.1747	0.0032	1033	38	1034	16	1038	18	99%	1033	38	Core
15G50-70	23	286	0.08	1.8001	0.0363	0.1751	0.0024	1054	35	1046	13	1040	13	99%	1054	35	Core
15G50-100	120	100	1.20	1.9911	0.0659	0.1885	0.0034	1117	69	1112	22	1113	19	99%	1117	69	Core
15G50-21	57	656	0.09	3.3964	0.1070	0.2350	0.0057	1722	47	1504	25	1361	30	90%	1722	47	Rim
15G50-25	36	44	0.82	3.5381	0.1488	0.2434	0.0071	1721	57	1536	33	1404	37	91%	1721	57	Rim
15G50-55	71	77	0.93	3.6489	0.1089	0.2574	0.0054	1661	48	1560	24	1476	28	94%	1661	48	Core
15G50-102	28	35	0.80	4.6584	0.1820	0.3085	0.0053	1787	61	1760	33	1733	26	98%	1787	61	Core
15G50-110	194	173	1.12	7.7908	0.2530	0.3723	0.0115	2366	34	2207	29	2040	54	92%	2366	34	Core
15G50-105	9	625	0.01	8.6179	0.2172	0.3841	0.0052	2483	33	2298	23	2096	24	90%	2483	33	Rim
15G50-77	283	238	1.19	7.1711	0.1533	0.3887	0.0063	2146	26	2133	19	2117	29	99%	2146	26	Core
15G50-54	75	163	0.46	8.9193	0.2282	0.4027	0.0076	2447	39	2330	23	2181	35	93%	2447	39	Core
15G50-30	505	174	2.91	9.6089	0.2453	0.4253	0.0083	2495	27	2398	24	2285	38	95%	2495	27	Core
15G50-57	10	10	0.98	12.3310	0.5028	0.4468	0.0065	2814	63	2630	38	2381	29	90%	2814	63	Core
15G50-93	210	95	2.22	10.0163	0.2688	0.4518	0.0083	2461	33	2436	25	2403	37	98%	2461	33	Core
15G50-85	86	78	1.09	10.5571	0.3488	0.4526	0.0118	2546	31	2485	31	2407	53	96%	2546	31	Core
15G50-58	33	26	1.25	11.0409	0.3439	0.4711	0.0086	2546	43	2527	29	2488	38	98%	2546	43	Core
15G50-42	67	129	0.52	12.4753	0.3180	0.4970	0.0090	2665	33	2641	24	2601	39	98%	2665	33	Core
15G50-96	48	115	0.42	12.2478	0.2856	0.4972	0.0075	2644	38	2624	22	2602	33	99%	2644	38	Core
15G50-32	101	41	2.49	21.3007	0.4467	0.5860	0.0083	3269	26	3152	20	2973	34	94%	3269	26	Core
15G50-114	96	474	0.20	21.9847	0.4207	0.5969	0.0086	3287	25	3183	19	3017	35	94%	3287	25	Rim
15G50-117	203	579	0.35	31.6158	0.7143	0.7153	0.0115	3569	30	3538	22	3478	43	98%	3569	30	Core
15G79, Garnet-bearing two mica schist																	
15G79-75	339	661	0.51	0.4651	0.0129	0.0633	0.0011	350	83	388	9	396	7	97%	396	7	Core
15G79-39	92	102	0.90	0.4830	0.0174	0.0643	0.0010	387	78	400	12	402	6	99%	402	6	Core
15G79-53	189	211	0.89	0.4895	0.0189	0.0652	0.0013	389	73	405	13	407	8	99%	407	8	Core
15G79-110	56	63	0.90	0.5085	0.0256	0.0656	0.0011	439	128	417	17	409	7	98%	409	7	Core
15G79-120	41	53	0.78	0.5283	0.0215	0.0660	0.0010	539	86	431	14	412	6	95%	412	6	Core
15G79-91	229	338	0.68	0.5134	0.0139	0.0669	0.0013	443	58	421	9	418	8	99%	418	8	Core
15G79-116	135	172	0.78	0.5430	0.0157	0.0672	0.0010	546	59	440	10	419	6	95%	419	6	Core
15G79-48	50	147	0.34	0.5137	0.0187	0.0675	0.0012	420	80	421	13	421	7	99%	421	7	Core
15G79-51	47	186	0.25	0.5146	0.0174	0.0675	0.0010	417	70	422	12	421	6	99%	421	6	Core
15G79-49	220	207	1.06	0.5275	0.0154	0.0678	0.0010	461	25	430	10	423	6	98%	423	6	Core
15G79-76	104	158	0.66	0.5070	0.0188	0.0680	0.0010	389	81	416	13	424	6	98%	424	6	Core
15G79-58	40	45	0.88	0.5142	0.0267	0.0682	0.0014	409	111	421	18	425	8	99%	425	8	Core
15G79-72	75	136	0.55	0.4979	0.0269	0.0684	0.0013	345	124	410	18	426	8	96%	426	8	Core
15G79-44	45	77	0.58	0.5247	0.0199	0.0689	0.0011	420	85	428	13	430	7	99%	430	7	Core
15G79-67	55	79	0.69	0.5348	0.0202	0.0690	0.0013	476	81	435	13	430	8	98%	430	8	Core
15G79-56	108	147	0.74	0.5037	0.0145	0.0691	0.0009	320	66	414	10	431	6	96%	431	6	Core
15G79-41	51	75	0.68	0.5332	0.0195	0.0696	0.0012	432	78	434	13	434	7	99%	434	7	Core
15G79-85	39	56	0.69	0.5519	0.0345	0.0709	0.0023	461	116	446	23	442	14	99%	442	14	Core
15G79-43	75	123	0.61	0.5823	0.0255	0.0712	0.0011	569	89	466	16	443	7	95%	443	7	Core
15G79-70	199	79	2.50	0.6030	0.0241	0.0784	0.0012	454	85	479	15	487	7	98%	487	7	Core
15G79-32	132	117	1.13	0.6046	0.0207	0.0788	0.0012	443	78	480	13	489	7	98%	489	7	Core
15G79-98	177	465	0.38	0.6890	0.0181	0.0837	0.0016	587	48	532	11	518	9	97%	518	9	Core
15G79-101	1	56	0.02	0.7455	0.0788	0.0839	0.0025	739	243	566	46	519	15	91%	519	15	Core
15G79-97	11	97	0.11	0.7309	0.0282	0.0885	0.0017	606	92	557	17	547	10	98%	547	10	Core
15G79-84	130	162	0.80	0.7114	0.0228	0.0888	0.0016	532	56	546	14	548	10	99%	548	10	Core
15G79-93	122	75	1.63	0.7733	0.0281	0.0918	0.0018	643	74	582	16	566	10	97%	566	10	Core
15G79-80	28	432	0.07	0.7582	0.0259	0.0944	0.0021	539	61	573	15	581	12	98%	581	12	Core
15G79-34	38	109	0.35	0.8082	0.0277	0.0977	0.0017	598	66	601	16	601	10	99%	601	10	Core
15G79-45	112	266	0.42	0.8333	0.0202	0.0979	0.0015	657	44	615	11	602	9	97%	602	9	Core
15G79-106	19	265	0.07	0.9111	0.0228	0.1043	0.0015	706	55	658	12	639	9	97%	639	9	Core
15G79-50	132	69	1.92	1.0141	0.0329	0.1142	0.0017	750	64	711	17	697	10	98%	697	10	Core
15G79-78	23	47	0.48	1.0068	0.0412	0.1164	0.0018	702	86	707	21	710	10	99%	710	10	Core
15G79-87	274	325	0.84	1.0630	0.0257	0.1205	0.0018	744	39	735	13	734	11	99%	734	11	Core
15G79-118	56	150	0.38	1.1104	0.0435	0.1206	0.0033	817	49	758	21	734	19	96%	734	19	Core
15G79-01	5	496	0.01	1.1208	0.0312	0.1237	0.0019	791	46	763	15	752	11	98%	752	11	Rim
15G79-55	105	83	1.27	1.0601	0.0290	0.1243	0.0018	733	56	734	14	755	10	97%	755	10	Core
15G79-119	106	183	0.58	1.1455	0.0304	0.1251	0.0021	818	45	775	14	760	12	98%	760	12	Core
15G79-73	31	69	0.45	1.1803	0.0412	0.1301	0.0021	1200	59	791	19	788	12	99%	788	12	Core
15G79-88	96	395	0.24	1.3293	0.0443	0.1322	0.0040	1009	42	859	19	801	23	93%	801	23	Core
15G79-03	19	443	0.04	1.3047	0.0269	0.1362	0.0016	922	40	848	12	823	9	97%	823	9	Rim
15G79-90	59	128	0.46	1.2980	0.0345	0.1398	0.0019	843	44	845	15	843	11	99%	843	11	Core
15G79-82	53	69	0.77	1.2574	0.0679	0.1399	0.0043	746	67	827	31	844	24	97%	844	24	Core
15G79-83	89	292	0.31	1.2844	0.0342	0.1404	0.0023	813	50	839	15	847	13	99%	847	13	Core

Continued Table 3

Grain No.	Element (ppm)		Th/U					Age (Ma)						Concor	Used ages		Postion
	Th	U		$^{207}Pb/^{235}U$	1σ	$^{206}Pb/^{238}U$	1σ	$^{207}Pb/^{206}Pb$	1σ	$^{207}Pb/^{235}U$	1σ	$^{206}Pb/^{238}U$	1σ				
15G79-65	89	197	0.45	1.3335	0.0417	0.1407	0.0027	889	81	860	18	849	15	98%	849	15	Core
15G79-107	160	280	0.57	1.3946	0.0344	0.1415	0.0020	967	52	887	15	853	11	96%	853	11	Core
15G79-104	106	158	0.67	1.3243	0.0411	0.1433	0.0028	826	57	856	18	863	16	99%	863	16	Core
15G79-92	75	427	0.18	1.3580	0.0330	0.1449	0.0023	865	42	871	14	872	13	99%	872	13	Core
15G79-68	94	492	0.19	1.3785	0.0380	0.1460	0.0027	883	33	880	16	879	15	99%	879	15	Core
15G79-37	32	21	1.54	1.3898	0.0553	0.1461	0.0031	902	84	885	23	879	18	99%	879	18	Core
15G79-62	75	122	0.61	1.3880	0.0451	0.1463	0.0028	900	54	884	19	880	16	99%	880	16	Core
15G79-64	132	138	0.95	1.4220	0.0403	0.1478	0.0023	920	48	898	17	888	13	98%	888	13	Core
15G79-117	124	136	0.91	1.5077	0.0401	0.1478	0.0026	1039	50	933	16	889	15	95%	889	15	Core
15G79-38	56	32	1.75	1.5722	0.0589	0.1579	0.0022	987	74	959	23	945	12	98%	945	12	Core
15G79-40	126	220	0.57	1.5454	0.0459	0.1582	0.0029	939	47	949	18	947	16	99%	947	16	Core
15G79-89	55	127	0.44	1.5224	0.0386	0.1585	0.0026	917	45	939	16	948	14	99%	948	14	Core
15G79-54	103	93	1.11	1.5655	0.0443	0.1609	0.0025	943	46	957	18	962	14	99%	962	14	Core
15G79-94	50	252	0.20	1.6621	0.0412	0.1658	0.0024	998	36	994	16	989	13	99%	989	13	Core
15G79-28	45	179	0.25	1.6645	0.0608	0.1718	0.0056	937	48	995	23	1022	31	97%	937	48	Rim
15G79-57	12	27	0.44	1.7667	0.0630	0.1732	0.0028	1028	57	1033	23	1030	15	99%	1028	57	Core
15G79-112	118	148	0.80	1.8344	0.0459	0.1735	0.0031	1106	48	1058	16	1031	17	97%	1106	48	Core
15G79-111	42	29	1.47	1.7702	0.0698	0.1741	0.0035	1029	81	1035	26	1035	19	99%	1029	81	Core
15G79-113	42	56	0.75	1.8476	0.0582	0.1761	0.0027	1089	63	1063	21	1045	15	98%	1089	63	Core
15G79-42	8	286	0.03	1.9184	0.0439	0.1820	0.0025	1102	43	1088	15	1078	14	99%	1102	43	Core
15G79-114	88	85	1.03	1.9610	0.0507	0.1826	0.0031	1139	50	1102	17	1081	17	98%	1139	50	Core
15G79-46	55	128	0.43	2.0739	0.0489	0.1922	0.0032	1152	40	1140	16	1133	18	99%	1152	40	Core
15G79-74	132	94	1.40	2.7605	0.0882	0.2242	0.0040	1411	45	1345	24	1304	21	96%	1411	45	Core
15G79-36	121	130	0.93	2.6610	0.0615	0.2246	0.0034	1331	38	1318	17	1306	18	99%	1331	38	Core
15G79-77	138	235	0.59	3.1575	0.0780	0.2560	0.0040	1417	38	1447	19	1469	21	98%	1417	38	Core
15G79-52	127	132	0.96	3.5388	0.0959	0.2631	0.0051	1573	34	1536	21	1506	26	98%	1573	34	Core
15G79-33	107	190	0.56	3.5811	0.0918	0.2665	0.0040	1572	41	1545	20	1523	20	98%	1572	41	Core
15G79-103	55	97	0.57	3.9741	0.1125	0.2703	0.0041	1731	54	1629	23	1542	21	94%	1731	54	Core
15G79-100	55	54	1.03	3.8077	0.1060	0.2787	0.0041	1598	53	1594	22	1585	21	99%	1598	53	Core
15G79-86	73	50	1.46	4.1159	0.1153	0.2899	0.0046	1673	44	1657	23	1641	23	98%	1673	44	Core
15G79-105	69	185	0.37	4.5871	0.1248	0.2941	0.0054	1840	46	1747	23	1662	27	95%	1840	46	Core
15G79-109	2	9	0.23	5.6262	0.1840	0.3165	0.0056	2077	61	1920	28	1772	27	92%	2077	61	Core
15G79-96	48	47	1.01	5.0148	0.1638	0.3172	0.0057	1933	46	1822	28	1776	28	97%	1933	46	Core
15G79-115	36	88	0.41	5.1047	0.1238	0.3261	0.0056	1848	35	1837	21	1820	27	99%	1848	35	Core
15G79-69	39	59	0.66	5.1249	0.1493	0.3377	0.0080	1810	37	1840	25	1875	38	98%	1810	37	Core
15G79-66	58	106	0.55	5.7141	0.1579	0.3426	0.0057	1972	38	1934	24	1899	28	98%	1972	38	Core
15G79-59	18	159	0.11	6.6289	0.1458	0.3695	0.0045	2098	35	2063	19	2027	21	98%	2098	35	Core
15G79-99	55	75	0.73	8.9622	0.2228	0.4108	0.0064	2429	35	2334	23	2219	29	94%	2429	35	Core
15G79-31	65	56	1.15	9.1480	0.2537	0.4201	0.0065	2432	43	2353	25	2261	30	96%	2432	43	Core
15G79-71	38	86	0.44	9.3651	0.3031	0.4218	0.0077	2473	41	2374	30	2269	35	95%	2473	41	Core
15G79-61	50	143	0.35	9.1789	0.2343	0.4223	0.0060	2431	39	2356	23	2271	27	96%	2431	39	Core
15G79-79	36	25	1.45	9.3397	0.2460	0.4230	0.0069	2461	42	2372	24	2274	31	95%	2461	42	Core
15G79-60	102	139	0.73	9.0724	0.1886	0.4252	0.0050	2398	31	2345	19	2284	23	97%	2398	31	Core
15G79-102	70	117	0.59	11.7063	0.3921	0.4376	0.0079	2765	50	2581	31	2340	35	90%	2765	50	Core
15G79-27	120	254	0.47	9.7273	0.2571	0.4393	0.0075	2451	29	2409	24	2347	34	97%	2451	29	Rim
15G79-63	18	29	0.64	10.2613	0.2687	0.4595	0.0069	2480	39	2459	24	2437	30	99%	2480	39	Core
15G79-47	126	141	0.90	10.4936	0.2135	0.4619	0.0072	2503	31	2479	19	2448	32	98%	2503	31	Core
15G79-35	5	14	0.38	10.2008	0.3188	0.4730	0.0095	2417	48	2453	29	2497	41	98%	2417	48	Core
15G79-108	61	77	0.80	14.2409	0.3337	0.5045	0.0081	2854	32	2766	22	2633	35	95%	2854	32	Core
15G79-95	122	428	0.28	14.1600	0.4241	0.5330	0.0133	2759	28	2760	28	2754	56	99%	2759	28	Core
15G79-81	45	74	0.60	19.2244	0.4753	0.5986	0.0085	3068	38	3053	24	3024	34	99%	3068	38	Core
15G57, Garnet-bearing two mica schist																	
15G57-24	62	396	0.16	0.5532	0.0388	0.0682	0.0040	567	74	447	25	425	24	94%	425	24	Rim
15G57-04	62	134	0.46	0.6248	0.0317	0.0748	0.0034	633	57	493	20	465	20	94%	465	20	Rim
15G57-112	50	177	0.28	0.6680	0.0229	0.0794	0.0020	639	53	519	14	493	12	94%	493	12	Core
15G57-115	120	413	0.29	0.7047	0.0265	0.0817	0.0023	680	41	542	16	506	14	93%	506	14	Core
15G57-84	48	277	0.17	0.7297	0.0228	0.0821	0.0013	746	258	556	13	509	8	91%	509	8	Core
15G57-07	181	285	0.64	0.7503	0.0361	0.0852	0.0034	728	56	568	21	527	20	92%	527	20	Rim
15G57-89	51	50	1.03	0.7739	0.0325	0.0929	0.0012	609	87	582	19	573	7	98%	573	7	Core
15G57-103	102	241	0.42	0.8444	0.0252	0.0941	0.0018	761	42	622	14	580	11	93%	580	11	Core
15G57-116	170	310	0.55	0.8527	0.0158	0.0969	0.0011	733	35	626	9	596	6	95%	596	6	Core
15G57-34	87	99	0.88	0.9115	0.0401	0.0981	0.0027	831	65	658	21	603	16	91%	603	16	Core
15G57-53	154	125	1.23	0.8763	0.0301	0.0996	0.0019	739	38	639	16	612	11	95%	612	11	Core
15G57-101	72	84	0.85	0.8667	0.0250	0.1012	0.0017	661	56	634	14	621	10	98%	621	10	Core
15G57-33	137	201	0.68	0.9048	0.0265	0.1015	0.0017	754	54	654	14	623	10	95%	623	10	Core
15G57-67	256	212	1.21	0.8689	0.0210	0.1028	0.0015	656	44	635	11	631	9	99%	631	9	Core
15G57-52	77	138	0.56	0.9259	0.0242	0.1032	0.0017	783	54	665	13	633	10	95%	633	10	Core
15G57-79	148	153	0.97	0.8723	0.0258	0.1047	0.0018	606	52	637	14	642	10	99%	642	10	Core
15G57-106	37	268	0.14	0.9840	0.0200	0.1054	0.0019	852	44	696	10	646	11	92%	646	11	Core
15G57-91	46	86	0.53	0.9171	0.0315	0.1081	0.0019	650	69	661	17	662	11	99%	662	11	Core
15G57-114	327	512	0.64	0.9730	0.0205	0.1094	0.0015	754	33	690	11	669	9	96%	669	9	Core
15G57-93	176	336	0.52	0.9827	0.0247	0.1094	0.0018	772	49	695	13	670	11	96%	670	11	Core

Continued Table 3

Grain No.	Element (ppm)		Th/U	$^{207}Pb/^{235}U$	1σ	$^{206}Pb/^{238}U$	1σ	Age (Ma)						Concor	Used ages		Postion
	Th	U						$^{207}Pb/^{206}Pb$	1σ	$^{207}Pb/^{235}U$	1σ	$^{206}Pb/^{238}U$	1σ				
15G57-102	283	528	0.53	0.9813	0.0198	0.1102	0.0015	750	43	694	10	674	9	97%	674	9	Core
15G57-94	43	76	0.57	0.9706	0.0359	0.1102	0.0027	731	65	689	18	674	16	97%	674	16	Core
15G57-117	70	73	0.96	0.9578	0.0307	0.1105	0.0017	698	64	682	16	676	10	99%	676	10	Core
15G57-55	56	34	1.66	0.9033	0.0518	0.1125	0.0021	550	133	653	28	687	12	94%	687	12	Core
15G57-63	232	349	0.66	1.0113	0.0274	0.1146	0.0023	743	49	710	14	699	13	98%	699	13	Core
15G57-81	85	121	0.70	1.0427	0.0358	0.1159	0.0030	776	58	725	18	707	17	97%	707	17	Core
15G57-31	73	47	1.53	1.0745	0.0581	0.1160	0.0028	856	109	741	28	708	16	95%	708	16	Core
15G57-69	100	66	1.52	1.0583	0.0420	0.1161	0.0017	806	77	733	21	708	10	96%	708	10	Core
15G57-37	33	29	1.14	1.0616	0.0403	0.1167	0.0017	798	78	735	20	712	10	96%	712	10	Core
15G57-109	170	206	0.83	1.0509	0.0240	0.1176	0.0019	761	37	729	12	717	11	98%	717	11	Core
15G57-86	66	61	1.08	1.0455	0.0277	0.1184	0.0020	744	56	727	14	722	11	99%	722	11	Core
15G57-95	165	120	1.37	1.1275	0.0353	0.1187	0.0016	887	55	767	17	723	9	94%	723	9	Core
15G57-72	82	75	1.09	1.1308	0.0368	0.1188	0.0021	899	64	768	18	724	12	94%	724	12	Core
15G57-75	93	98	0.95	1.0893	0.0333	0.1188	0.0022	817	56	748	16	724	13	96%	724	13	Core
15G57-80	110	148	0.74	1.0509	0.0276	0.1192	0.0020	731	53	729	14	726	11	99%	726	11	Core
15G57-62	106	181	0.59	1.0453	0.0289	0.1194	0.0018	724	28	727	14	727	10	99%	727	10	Core
15G57-88	99	163	0.61	1.0635	0.0294	0.1201	0.0020	743	46	736	14	731	12	99%	731	12	Core
15G57-56	184	235	0.79	1.1022	0.0238	0.1202	0.0016	833	47	754	11	732	9	96%	732	9	Core
15G57-76	69	78	0.89	1.0384	0.0290	0.1207	0.0019	687	57	723	14	734	11	98%	734	11	Core
15G57-119	113	132	0.86	1.0472	0.0262	0.1208	0.0018	698	43	727	13	735	10	98%	735	10	Core
15G57-46	141	133	1.06	1.1052	0.0451	0.1212	0.0041	817	76	756	22	738	24	97%	738	24	Core
15G57-22	74	409	0.18	1.0897	0.0262	0.1213	0.0019	783	52	748	13	738	11	98%	738	11	Rim
15G57-45	146	153	0.96	1.1385	0.0380	0.1221	0.0031	850	153	772	18	743	18	96%	743	18	Core
15G57-38	222	228	0.97	1.1231	0.0236	0.1225	0.0017	813	38	764	11	745	10	97%	745	10	Core
15G57-108	60	64	0.95	1.1106	0.0366	0.1228	0.0023	791	65	758	18	747	13	98%	747	13	Core
15G57-97	116	403	0.29	1.1293	0.0265	0.1228	0.0022	833	51	767	13	747	13	97%	747	13	Core
15G57-47	99	248	0.40	1.1623	0.0392	0.1230	0.0024	880	63	783	18	748	14	95%	748	14	Core
15G57-40	69	70	0.99	1.0573	0.0331	0.1232	0.0024	672	54	732	16	749	14	97%	749	14	Core
15G57-41	122	124	0.98	1.1489	0.0341	0.1235	0.0022	839	56	777	16	751	13	96%	751	13	Core
15G57-113	83	148	0.56	1.1303	0.0235	0.1247	0.0015	798	34	768	11	757	9	98%	757	9	Core
15G57-107	91	100	0.90	1.1513	0.0275	0.1247	0.0017	828	44	778	13	757	10	97%	757	10	Core
15G57-92	53	80	0.66	1.0918	0.0346	0.1247	0.0024	717	54	749	17	757	13	98%	757	13	Core
15G57-66	129	161	0.80	1.0936	0.0286	0.1249	0.0022	728	56	750	14	759	13	98%	759	13	Core
15G57-58	85	92	0.92	1.1491	0.0311	0.1252	0.0020	833	50	777	15	761	11	97%	761	11	Core
15G57-64	67	626	0.11	1.1601	0.0298	0.1253	0.0024	839	41	782	14	761	14	97%	761	14	Core
15G57-60	58	95	0.61	1.0441	0.0334	0.1256	0.0019	617	69	726	17	763	11	95%	763	11	Core
15G57-27	21	52	0.41	1.1286	0.0337	0.1258	0.0033	798	70	767	16	764	19	99%	764	19	Core
15G57-32	78	69	1.13	1.1834	0.0341	0.1267	0.0020	850	53	793	16	769	11	96%	769	11	Core
15G57-82	255	500	0.51	1.1860	0.0248	0.1270	0.0017	850	45	794	12	771	10	97%	771	10	Core
15G57-73	20	32	0.64	1.1754	0.0497	0.1276	0.0021	835	87	789	23	774	12	98%	774	12	Core
15G57-65	175	169	1.04	1.1897	0.0308	0.1279	0.0020	850	151	796	14	776	12	97%	776	12	Core
15G57-96	114	170	0.67	1.1685	0.0301	0.1284	0.0018	798	55	786	14	779	10	99%	779	10	Core
15G57-70	144	195	0.74	1.2777	0.0324	0.1285	0.0017	984	46	836	14	780	10	93%	780	10	Core
15G57-83	50	93	0.53	1.1754	0.0293	0.1290	0.0021	806	54	789	14	782	12	99%	782	12	Core
15G57-120	156	343	0.45	1.2156	0.0259	0.1297	0.0018	863	35	808	12	786	10	97%	786	10	Core
15G57-05	54	218	0.25	1.2409	0.0301	0.1324	0.0019	865	35	819	14	801	11	97%	801	11	Rim
15G57-42	100	313	0.32	1.2487	0.0296	0.1326	0.0025	872	46	823	13	803	14	97%	803	14	Core
15G57-48	72	223	0.33	1.2844	0.0312	0.1328	0.0021	931	46	839	14	804	12	95%	804	12	Core
15G57-118	84	115	0.73	1.2171	0.0303	0.1329	0.0018	817	46	808	14	804	10	99%	804	10	Core
15G57-74	109	195	0.56	1.2542	0.0326	0.1329	0.0023	880	46	825	15	805	13	97%	805	13	Core
15G57-77	163	326	0.50	1.2729	0.0317	0.1338	0.0024	900	39	834	14	810	14	97%	810	14	Core
15G57-54	119	171	0.69	1.2730	0.0365	0.1345	0.0022	887	50	834	16	813	13	97%	813	13	Core
15G57-44	114	128	0.90	1.2415	0.0345	0.1350	0.0023	820	50	820	16	816	13	99%	816	13	Core
15G57-19	59	124	0.48	1.2446	0.0314	0.1351	0.0020	831	49	821	14	817	11	99%	817	11	Rim
15G57-85	120	272	0.44	1.2546	0.0286	0.1352	0.0021	835	39	825	13	817	12	98%	817	12	Core
15G57-25	132	133	0.99	1.2790	0.0330	0.1367	0.0020	865	52	836	15	826	11	98%	826	11	Rim
15G57-59	87	228	0.38	1.3143	0.0343	0.1368	0.0024	920	43	852	15	827	14	96%	827	14	Core
15G57-16	51	148	0.34	1.2686	0.0315	0.1381	0.0020	833	51	832	14	834	11	99%	834	11	Rim
15G57-111	96	220	0.44	1.2645	0.0295	0.1383	0.0024	815	37	830	13	835	13	99%	835	13	Core
15G57-104	48	75	0.64	1.3258	0.0320	0.1388	0.0019	898	48	857	14	838	11	97%	838	11	Core
15G57-61	102	152	0.67	1.2458	0.0418	0.1401	0.0031	761	59	822	19	845	18	97%	845	18	Core
15G57-49	101	227	0.45	1.3595	0.0320	0.1403	0.0020	1000	38	872	14	846	11	97%	846	11	Core
15G57-39	22	43	0.50	1.3426	0.0520	0.1405	0.0024	895	72	864	23	848	14	98%	848	14	Core
15G57-105	159	350	0.45	1.3648	0.0301	0.1429	0.0022	894	37	874	13	861	12	98%	861	12	Core
15G57-51	63	114	0.55	1.4133	0.0417	0.1430	0.0022	989	54	895	18	862	13	96%	862	13	Core
15G57-43	111	252	0.44	1.4048	0.0363	0.1439	0.0025	940	45	891	15	867	14	97%	867	14	Core
15G57-29	28	33	0.84	1.3357	0.0594	0.1440	0.0025	850	85	861	26	867	14	99%	867	14	Rim
15G57-71	86	139	0.62	1.3962	0.0464	0.1475	0.0023	887	75	887	20	887	13	99%	887	13	Core
15G57-09	25	50	0.51	1.5756	0.0440	0.1515	0.0018	1076	54	961	17	909	10	94%	909	10	Rim
15G57-90	62	101	0.62	2.0734	0.0530	0.1944	0.0026	1121	44	1140	18	1145	14	99%	1121	44	Core
15G57-99	62	63	0.98	4.2318	0.0822	0.2843	0.0034	1755	34	1680	16	1613	17	95%	1755	34	Core
15G57-14	113	263	0.43	4.4127	0.0940	0.2900	0.0047	1811	33	1715	18	1642	24	95%	1811	33	Rim

Continued Table 3

Grain No.	Element (ppm)		Th/U					Age (Ma)						Concor	Used ages		Postion
	Th	U		^{207}Pb/^{235}U	1σ	^{206}Pb/^{238}U	1σ	^{207}Pb/^{206}Pb	1σ	^{207}Pb/^{235}U	1σ	^{206}Pb/^{238}U	1σ				
15G57-87	34	32	1.08	4.4456	0.1165	0.3047	0.0046	1716	39	1721	22	1715	23	99%	1716	39	Core
15G57-21	145	162	0.89	4.5908	0.1174	0.3052	0.0053	1787	40	1748	21	1717	26	98%	1787	40	Rim
15G57-68	54	66	0.82	5.2788	0.1393	0.3353	0.0047	1865	44	1865	23	1864	23	99%	1865	44	Core
15G57-110	31	84	0.37	8.7326	0.1793	0.3939	0.0060	2457	24	2310	19	2141	28	92%	2457	24	Core
15G03, Garnet-sillimanite gneiss																	
15G03-82	175	680	0.26	0.5492	0.0209	0.0665	0.0012	600	83	444	14	415	7	93%	415	7	Core
15G03-10	778	318	2.45	0.6085	0.0265	0.0715	0.0015	676	96	483	17	445	9	91%	445	9	Rim
15G03-117	62	163	0.38	0.6547	0.0314	0.0723	0.0022	792	94	511	19	450	14	~~87%~~			
15G03-101	76	718	0.11	0.7052	0.0252	0.0759	0.0019	806	57	542	15	471	12	~~86%~~			
15G03-71	219	396	0.55	0.6257	0.0215	0.0772	0.0013	600	72	493	13	479	8	97%	479	8	Core
15G03-74	144	179	0.81	0.6195	0.0266	0.0777	0.0020	522	84	490	17	483	12	98%	483	12	Core
15G03-53	323	584	0.55	0.6259	0.0252	0.0798	0.0016	465	77	494	16	495	9	99%	495	9	Core
15G03-81	217	127	1.71	0.6499	0.0340	0.0801	0.0022	569	114	508	21	497	13	97%	497	13	Core
15G03-35	146	690	0.21	0.5898	0.0640	0.0811	0.0034	213	248	471	41	503	21	93%	503	21	Core
15G03-89	32	86	0.38	0.6311	0.0341	0.0815	0.0019	454	122	497	21	505	11	98%	505	11	Core
15G03-96	339	556	0.61	0.6204	0.0191	0.0815	0.0015	398	69	490	12	505	9	96%	505	9	Core
15G03-66	37	127	0.29	0.7026	0.0293	0.0817	0.0017	680	89	540	17	506	10	93%	506	10	Core
15G03-11	122	126	0.97	0.7262	0.0334	0.0820	0.0017	746	91	554	20	508	10	91%	508	10	Rim
15G03-80	328	282	1.16	0.6865	0.0309	0.0823	0.0019	598	102	531	19	510	11	96%	510	11	Core
15G03-70	259	411	0.63	0.6448	0.0190	0.0825	0.0014	457	63	505	12	511	9	98%	511	9	Core
15G03-13	269	267	1.01	0.6903	0.0268	0.0827	0.0019	620	76	533	16	512	12	96%	512	12	Rim
15G03-16	179	286	0.63	0.6863	0.0205	0.0845	0.0015	546	61	531	12	523	9	98%	523	9	Rim
15G03-84	28	557	0.05	0.7791	0.0253	0.0849	0.0015	765	68	585	14	525	9	~~89%~~			
15G03-86	81	202	0.40	0.6608	0.0260	0.0871	0.0016	409	98	515	16	539	9	95%	539	9	Core
15G03-39	61	161	0.38	0.7984	0.0439	0.0882	0.0027	787	117	596	25	545	16	91%	545	16	Core
15G03-61	18	269	0.07	0.7164	0.0243	0.0889	0.0019	522	61	549	14	549	11	99%	549	11	Core
15G03-102	207	267	0.78	0.6729	0.0230	0.0891	0.0015	387	78	522	14	550	9	94%	550	9	Core
15G03-116	145	368	0.39	0.7314	0.0294	0.0893	0.0022	528	81	557	17	552	13	98%	552	13	Core
15G03-106	197	140	1.41	0.7043	0.0279	0.0894	0.0019	498	89	541	17	552	11	98%	552	11	Core
15G03-109	112	367	0.31	0.7197	0.0239	0.0894	0.0016	494	64	551	14	552	9	99%	552	9	Core
15G03-105	178	545	0.33	0.7453	0.0200	0.0895	0.0014	583	59	565	12	553	8	97%	553	8	Core
15G03-4	31	68	0.45	0.7849	0.0327	0.0900	0.0017	731	90	588	19	555	10	94%	555	10	Rim
15G03-76	185	80	2.31	0.7403	0.0365	0.0902	0.0020	591	113	563	21	556	12	98%	556	12	Core
15G03-18	260	320	0.81	0.8384	0.0283	0.0906	0.0017	817	66	618	16	559	10	~~89%~~			
15G03-9	68	293	0.23	0.8290	0.0519	0.0912	0.0046	772	75	613	29	563	27	91%	563	27	Rim
15G03-5	122	372	0.33	0.8664	0.0256	0.0914	0.0016	865	58	634	14	564	9	~~88%~~			
15G03-6	144	369	0.39	0.8007	0.0280	0.0967	0.0037	656	74	597	16	595	22	99%	595	22	Core
15G03-55	302	433	0.70	0.7798	0.0281	0.0992	0.0019	480	50	585	16	610	11	95%	610	11	Core
15G03-75	20	92	0.22	0.9071	0.0446	0.1017	0.0023	791	113	656	24	624	13	95%	624	13	Core
15G03-43	115	214	0.54	1.0060	0.0349	0.1021	0.0023	924	59	707	18	627	13	~~88%~~			
15G03-49	34	147	0.23	0.9601	0.0347	0.1039	0.0021	831	76	683	18	637	12	93%	637	12	Core
15G03-25	305	306	0.99	0.7670	0.0596	0.1045	0.0021	272	206	578	34	641	12	~~89%~~			
15G03-90	143	351	0.41	0.8920	0.0295	0.1058	0.0019	591	70	647	16	648	11	99%	648	11	Core
15G03-12	115	796	0.14	1.0434	0.0291	0.1082	0.0017	906	53	726	14	662	10	90%	662	10	Core
15G03-115	30	619	0.05	1.1090	0.0386	0.1095	0.0027	959	54	758	19	670	16	~~87%~~			
15G03-27	98	281	0.35	0.8539	0.0900	0.1105	0.0026	387	280	627	49	676	15	92%	676	15	Core
15G03-91	1065	179	5.95	1.0405	0.0391	0.1118	0.0023	854	118	724	19	683	13	94%	683	13	Core
15G03-54	57	123	0.47	0.9860	0.0502	0.1138	0.0027	740	114	697	26	695	16	99%	695	16	Core
15G03-112	364	237	1.54	1.0698	0.0371	0.1163	0.0018	776	79	739	18	709	11	95%	709	11	Core
15G03-88	77	125	0.62	1.0726	0.0477	0.1235	0.0024	657	94	740	23	750	14	98%	750	14	Core
15G03-57	58	74	0.79	1.0606	0.0707	0.1271	0.0048	754	160	734	35	772	27	95%	772	27	Core
15G03-45	63	55	1.16	1.1687	0.0568	0.1273	0.0031	843	101	786	27	772	17	98%	772	17	Core
15G03-67	113	105	1.08	1.2380	0.0644	0.1273	0.0029	972	115	818	29	773	17	94%	773	17	Core
15G03-65	67	275	0.24	1.2420	0.0340	0.1275	0.0023	920	48	820	15	773	13	94%	773	13	Core
15G03-110	163	345	0.47	1.1908	0.0402	0.1275	0.0021	817	70	796	19	774	12	97%	774	12	Core
15G03-42	135	228	0.59	1.1987	0.0352	0.1277	0.0025	843	59	800	16	775	14	96%	775	14	Core
15G03-41	94	55	1.70	1.2266	0.0600	0.1278	0.0034	906	-94	813	27	775	20	95%	775	20	Core
15G03-37	65	84	0.78	1.1115	0.0917	0.1281	0.0030	639	199	759	44	777	17	97%	777	17	Core
15G03-63	174	501	0.35	1.2717	0.0350	0.1281	0.0024	967	49	833	16	777	14	93%	777	14	Core
15G03-103	162	120	1.34	1.2038	0.0416	0.1301	0.0028	817	65	802	19	788	16	98%	788	16	Core
15G03-28	132	315	0.42	1.0623	0.1295	0.1302	0.0040	498	318	735	64	789	23	92%	789	23	Rim
15G03-92	9	17	0.56	1.4036	0.1740	0.1348	0.0075	1476	283	890	73	815	42	91%	815	42	Core
15G03-26	2	404	0.005	1.1813	0.1068	0.1385	0.0033	598	228	792	50	836	19	94%	836	19	Rim
15G03-1	29	53	0.54	1.2855	0.0574	0.1391	0.0032	831	96	839	26	840	18	99%	840	18	Rim
15G03-15	127	202	0.63	1.3857	0.0403	0.1398	0.0024	969	55	883	17	844	13	95%	844	13	Rim
15G03-83	211	213	0.99	1.3400	0.0486	0.1402	0.0025	861	74	863	21	846	14	97%	846	14	Core
15G03-19	41	279	0.15	1.3782	0.0438	0.1404	0.0027	946	62	880	19	847	15	96%	847	15	Rim
15G03-85	50	77	0.65	1.3542	0.0707	0.1418	0.0037	950	117	869	30	855	21	98%	855	21	Core
15G03-108	177	171	1.03	1.4312	0.0414	0.1442	0.0022	950	63	902	17	869	13	96%	869	13	Core
15G03-34	527	417	1.27	1.1545	0.1372	0.1458	0.0037	428	305	779	65	877	21	~~88%~~			Core
15G03-69	113	240	0.47	1.4899	0.0421	0.1464	0.0025	1011	49	926	17	881	14	94%	881	14	Core
15G03-60	113	119	0.95	1.4663	0.0790	0.1506	0.0041	943	104	917	33	905	23	98%	905	23	Core

Continued Table 3

Grain No.	Element (ppm)		Th/U	$^{207}Pb/^{235}U$	1σ	$^{206}Pb/^{238}U$	1σ	Age (Ma)						Concor	Used ages		Postion
	Th	U						$^{207}Pb/^{206}Pb$	1σ	$^{207}Pb/^{235}U$	1σ	$^{206}Pb/^{238}U$	1σ				
15G03-104	28	73	0.39	1.5202	0.0657	0.1523	0.0035	983	119	939	26	914	20	97%	914	20	Core
15G03-7	600	1122	0.53	1.6406	0.0429	0.1527	0.0027	1124	46	986	17	916	15	92%	916	15	Rim
15G03-78	41	83	0.49	1.6274	0.0731	0.1622	0.0033	1011	96	981	28	969	18	98%	969	18	Core
15G03-47	52	95	0.55	1.7619	0.0711	0.1671	0.0035	1106	78	1032	26	996	19	96%	996	19	Core
15G03-94	59	200	0.29	1.7032	0.0527	0.1694	0.0029	991	64	1010	20	1009	16	99%	991	64	Core
15G03-107	110	302	0.36	1.8042	0.0519	0.1742	0.0031	1031	56	1047	19	1035	17	98%	1031	56	Rim
15G03-51	162	224	0.72	1.8595	0.0718	0.1784	0.0034	1057	71	1067	26	1058	19	99%	1057	71	Core
15G03-46	82	236	0.35	1.9920	0.0581	0.1896	0.0034	1061	50	1113	20	1119	19	99%	1061	50	Core
15G03-77	366	873	0.42	1.9188	0.0531	0.1775	0.0029	1109	54	1088	18	1053	16	96%	1109	54	Core
15G03-59	104	179	0.58	2.5109	0.1069	0.2199	0.0050	1250	80	1275	31	1281	26	99%	1250	80	Core
15G03-87	314	400	0.78	3.7102	0.1040	0.2704	0.0049	1561	48	1574	22	1543	25	98%	1561	48	Core
15G03-8	73	127	0.58	4.1507	0.1219	0.2688	0.0046	1820	50	1664	24	1535	23	91%	1820	50	Rim
15G03-73	86	423	0.20	3.9129	0.0973	0.2461	0.0036	1856	42	1616	20	1418	18	~~86%~~			Core
15G03-3	56	66	0.85	4.8626	0.1392	0.3088	0.0058	1861	56	1796	24	1735	28	96%	1861	56	Rim
15G03-52	120	234	0.51	6.4712	0.1947	0.3630	0.0069	2065	47	2042	26	1996	33	97%	2065	47	Core
15G03-98	181	383	0.47	6.3647	0.1730	0.3128	0.0059	2288	44	2027	24	1754	29	~~85%~~			Core
15G03-56	138	248	0.56	7.3372	0.2198	0.3437	0.0063	2377	48	2153	27	1905	30	~~87%~~			Core
15G03-100	222	239	0.93	10.2612	0.2686	0.4648	0.0074	2420	40	2459	24	2461	33	99%	2420	40	Core
15G03-99	73	87	0.84	11.0049	0.3690	0.5005	0.0119	2428	50	2524	31	2616	51	96%	2428	50	Core
15G03-95	211	143	1.48	9.4388	0.2660	0.4243	0.0086	2439	42	2382	26	2280	39	95%	2439	42	Core
15G03-118	113	146	0.77	8.5925	0.2492	0.3815	0.0071	2442	47	2296	26	2083	33	90%	2442	47	Core
15G03-93	102	207	0.49	9.4492	0.2422	0.4231	0.0075	2444	41	2383	24	2274	34	95%	2444	41	Core
15G03-58	484	249	1.95	9.5062	0.3100	0.4283	0.0085	2446	54	2388	30	2298	38	96%	2446	54	Core
15G03-62	41	37	1.10	10.3403	0.3356	0.4749	0.0122	2448	50	2466	30	2505	53	98%	2448	50	Core
15G03-114	247	419	0.59	7.8892	0.2011	0.3481	0.0054	2454	42	2218	23	1925	26	~~85%~~			Core
15G03-113	244	128	1.91	9.3762	0.2472	0.4128	0.0065	2465	46	2376	24	2228	29	93%	2465	46	Core
15G03-68	67	88	0.75	8.9573	0.2185	0.3977	0.0064	2480	42	2334	22	2158	30	92%	2480	42	Core
15G03-79	413	384	1.08	10.1049	0.2954	0.4390	0.0076	2484	49	2444	27	2346	34	95%	2484	49	Core
15G03-44	124	223	0.55	9.9616	0.2218	0.4293	0.0066	2507	35	2431	21	2303	30	94%	2507	35	Core
15G03-72	68	111	0.61	9.6158	0.2876	0.4130	0.0083	2521	44	2399	28	2229	38	92%	2521	44	Core
15G03-64	51	92	0.55	9.5642	0.2049	0.4126	0.0065	2521	33	2394	20	2227	30	92%	2521	33	Core
15G03-50	80	310	0.26	11.1839	0.3180	0.4803	0.0085	2522	44	2539	27	2529	37	99%	2522	44	Core
15G03-119	336	493	0.68	10.7192	0.2824	0.4246	0.0068	2631	43	2499	25	2281	31	90%	2631	43	Core
15G03-48	30	63	0.48	11.8514	0.3484	0.4213	0.0075	2839	45	2593	28	2266	34	~~86%~~			Core
15G06,Garnet-sillimanite gneiss																	
15G06-39	86	1674	0.05	0.4128	0.0124	0.0490	0.0007	611	101	351	9	308	4	~~87%~~			Core
15G06-116	108	226	0.48	0.4223	0.0229	0.0562	0.0022	439	130	358	16	352	13	98%	352	13	Core
15G06-43	193	124	1.56	0.4841	0.0319	0.0657	0.0020	367	152	401	22	410	12	97%	410	12	Core
15G06-47	146	216	0.68	0.5420	0.0271	0.0673	0.0012	561	117	440	18	420	8	95%	420	8	Core
15G06-25	105	468	0.23	0.6140	0.0224	0.0707	0.0013	733	78	486	14	440	8	90%	440	8	Core
15G06-29	48	314	0.15	0.5891	0.0316	0.0719	0.0017	583	120	470	20	448	10	95%	448	10	Rim
15G06-6	171	325	0.53	0.6096	0.0170	0.0760	0.0012	520	66	483	11	472	7	97%	472	7	Core
15G06-50	477	566	0.84	0.6382	0.0224	0.0764	0.0015	594	70	501	14	475	9	94%	475	9	Core
15G06-41	329	504	0.65	0.6425	0.0308	0.0764	0.0015	591	108	504	19	475	9	94%	475	9	Core
15G06-120	13	66	0.20	0.6173	0.0429	0.0796	0.0020	443	157	488	27	494	12	98%	494	12	Core
15G06-105	361	295	1.23	0.6033	0.0214	0.0797	0.0017	394	79	479	14	494	10	96%	494	10	Core
15G06-72	58	75	0.77	0.7094	0.0495	0.0807	0.0020	809	172	544	29	501	12	91%	501	12	Core
15G06-48	247	178	1.39	0.6437	0.0314	0.0809	0.0021	600	113	505	19	501	13	99%	501	13	Core
15G06-110	150	320	0.47	0.6647	0.0256	0.0812	0.0017	567	83	517	16	503	10	97%	503	10	Core
15G06-101	190	103	1.84	0.7381	0.0351	0.0813	0.0017	787	91	561	21	504	10	~~89%~~			Core
15G06-98	183	93	1.97	0.6506	0.0273	0.0816	0.0015	509	97	509	17	506	9	99%	506	9	Core
15G06-15	157	100	1.56	0.6733	0.0253	0.0827	0.0016	561	81	523	15	512	9	98%	512	9	Core
15G06-70	138	938	0.15	0.6806	0.0319	0.0832	0.0026	543	89	527	19	515	15	97%	515	15	Core
15G06-118	43	450	0.10	0.7396	0.0375	0.0835	0.0031	635	78	562	22	517	18	91%	517	18	Core
15G06-9	151	438	0.34	0.6842	0.0201	0.0839	0.0012	554	57	529	12	519	7	98%	519	7	Rim
15G06-68	527	817	0.65	0.6915	0.0216	0.0842	0.0015	554	75	534	13	521	9	97%	521	9	Core
15G06-24	32	387	0.08	0.7669	0.0383	0.0843	0.0026	754	51	578	22	522	15	~~89%~~			Rim
15G06-64	224	491	0.46	0.7047	0.0272	0.0844	0.0021	554	78	542	16	522	12	96%	522	12	Core
15G06-109	237	310	0.77	0.6906	0.0260	0.0850	0.0017	543	80	533	16	526	10	98%	526	10	Core
15G06-44	240	246	0.97	0.8042	0.0353	0.0852	0.0019	862	94	599	20	527	11	~~87%~~			Core
15G06-61	9	234	0.04	0.7438	0.0337	0.0861	0.0018	637	106	565	20	532	10	94%	532	10	White
15G06-34	85	191	0.44	0.7715	0.0269	0.0871	0.0015	706	71	581	15	538	9	92%	538	9	Core
15G06-37	42	665	0.06	0.8670	0.0267	0.0883	0.0014	920	65	634	15	546	8	~~85%~~	546	8	Rim
15G06-100	59	75	0.79	0.8537	0.0349	0.0949	0.0021	794	91	627	19	585	12	93%	585	12	Core
15G06-26	45	120	0.37	0.8428	0.0453	0.1021	0.0025	576	131	621	25	627	15	99%	627	15	Rim
15G06-74	85	185	0.46	0.8638	0.0374	0.1025	0.0019	635	91	632	20	629	11	99%	629	11	Core
15G06-3	30	293	0.10	0.8948	0.0257	0.1042	0.0016	665	59	649	14	639	9	98%	639	9	Rim
15G06-113	263	246	1.07	1.0197	0.0360	0.1109	0.0021	798	78	714	18	678	12	94%	678	12	Core
15G06-78	151	210	0.72	1.0048	0.0314	0.1152	0.0022	722	64	706	16	703	13	99%	703	13	Core
15G06-18	150	722	0.21	1.1256	0.0300	0.1168	0.0020	894	54	766	14	712	11	92%	712	11	Core
15G06-99	83	173	0.48	1.0318	0.0306	0.1182	0.0021	709	66	720	15	720	12	99%	720	12	Core
15G06-93	47	104	0.45	1.0628	0.0380	0.1215	0.0023	698	76	735	19	739	13	99%	739	13	Core

Continued Table 3

Grain No.	Element (ppm)		Th/U	^{207}Pb/^{235}U	1σ	^{206}Pb/^{238}U	1σ	Age (Ma)						Concor	Used ages		Postion
	Th	U						^{207}Pb/^{206}Pb	1σ	^{207}Pb/^{235}U	1σ	^{206}Pb/^{238}U	1σ				
15G06-90	70	231	0.30	1.2060	0.0394	0.1231	0.0026	928	61	803	18	749	15	92%	749	15	Core
15G06-7	176	388	0.45	1.2989	0.0327	0.1273	0.0021	1017	43	845	14	773	12	91%	773	12	Rim
15G06-20	63	1276	0.05	1.2213	0.0337	0.1274	0.0020	865	56	810	15	773	12	95%	773	12	Rim
15G06-12	77	163	0.48	1.2850	0.0479	0.1275	0.0028	1013	73	839	21	774	16	91%	774	16	Rim
15G06-51	330	657	0.50	1.3964	0.0451	0.1282	0.0026	1148	59	887	19	777	15	~~86%~~			Core
15G06-40	45	307	0.15	1.3761	0.0565	0.1293	0.0037	1083	69	879	24	784	21	~~88%~~			Core
15G06-62	71	644	0.11	1.4148	0.0584	0.1293	0.0034	1122	79	895	25	784	20	~~86%~~			Core
15G06-58	467	269	1.74	1.2939	0.0381	0.1303	0.0023	963	56	843	17	790	13	93%	790	13	Core
15G06-49	31	391	0.08	1.2986	0.0450	0.1317	0.0027	966	74	845	20	798	15	94%	798	15	Core
15G06-30	232	1094	0.21	1.2787	0.0406	0.1327	0.0022	887	70	836	18	803	12	95%	803	12	Rim
15G06-23	73	174	0.42	1.3409	0.0479	0.1347	0.0025	966	69	864	21	814	14	94%	814	14	Core
15G06-81	111	146	0.76	1.2569	0.0519	0.1355	0.0029	831	68	826	23	819	17	99%	819	17	Core
15G06-36	67	208	0.32	1.4230	0.0451	0.1371	0.0024	1035	64	899	19	828	13	91%	828	13	Core
15G06-53	434	460	0.94	1.3760	0.0359	0.1380	0.0020	969	52	879	15	833	12	94%	833	12	Core
15G06-55	138	477	0.29	1.3449	0.0378	0.1383	0.0020	915	54	865	16	835	11	96%	835	11	Core
15G06-42	166	290	0.57	1.4526	0.0622	0.1388	0.0033	1072	85	911	26	838	19	91%	838	19	Core
15G06-13	208	297	0.70	1.4063	0.0369	0.1405	0.0020	976	52	892	16	847	11	94%	847	11	Core
15G06-80	331	667	0.50	1.4678	0.0359	0.1487	0.0023	969	46	917	15	893	13	97%	893	13	Core
15G06-85	57	40	1.40	1.3748	0.0712	0.1508	0.0043	889	113	878	30	906	24	96%	906	24	Core
15G06-19	149	345	0.43	1.4728	0.0449	0.1529	0.0027	883	55	919	18	917	15	99%	917	15	Core
15G06-117	156	376	0.41	1.6824	0.0586	0.1540	0.0033	1117	69	1002	22	924	18	91%	924	18	Core
15G06-114	96	134	0.72	1.3869	0.0479	0.1542	0.0031	761	75	883	20	925	17	95%	925	17	Core
15G06-83	113	207	0.55	1.5218	0.0442	0.1569	0.0027	931	59	939	18	940	15	99%	940	15	Core
15G06-86	26	25	1.01	1.4398	0.0816	0.1595	0.0046	787	81	906	34	954	25	94%	954	25	Core
15G06-96	68	168	0.40	1.8810	0.0567	0.1608	0.0026	1277	56	1074	20	961	14	~~88%~~			Core
15G06-111	91	133	0.69	1.5826	0.0668	0.1609	0.0036	939	83	963	26	962	20	99%	962	20	Core
15G06-119	155	97	1.61	1.4676	0.0553	0.1614	0.0030	767	53	917	23	964	17	94%	964	17	Core
15G06-75	132	365	0.36	1.5737	0.0447	0.1614	0.0028	929	54	960	18	965	15	99%	965	15	Core
15G06-112	51	62	0.82	1.5673	0.0686	0.1624	0.0038	931	100	957	27	970	21	98%	970	21	Core
15G06-63	108	139	0.78	1.5956	0.0635	0.1636	0.0029	902	88	969	25	977	16	99%	977	16	Core
15G06-57	54	149	0.36	1.6696	0.0555	0.1640	0.0030	1039	67	997	21	979	17	98%	979	17	Core
15G06-11	157	207	0.76	1.6510	0.0595	0.1642	0.0040	983	54	990	23	980	22	98%	980	22	Core
15G06-77	426	670	0.64	1.6003	0.0390	0.1646	0.0025	924	46	970	15	982	14	98%	982	14	Core
15G06-8	27	108	0.25	1.6504	0.0569	0.1651	0.0030	1000	74	990	22	985	16	99%	985	16	Core
15G06-107	58	121	0.48	1.8095	0.0632	0.1791	0.0036	1006	38	1049	23	1062	20	98%	1006	38	Core
15G06-103	85	135	0.63	2.0002	0.0667	0.1917	0.0034	1072	64	1116	23	1131	18	98%	1072	64	Core
15G06-21	68	116	0.59	1.7902	0.0640	0.1682	0.0034	1100	72	1042	23	1002	19	96%	1100	72	Core
15G06-16	111	260	0.43	2.1308	0.0505	0.1955	0.0028	1139	44	1159	16	1151	15	99%	1139	44	Core
15G06-97	83	429	0.19	2.0593	0.0840	0.1749	0.0056	1255	46	1135	28	1039	31	91%	1255	46	Core
15G06-76	231	535	0.43	2.8045	0.0658	0.2246	0.0031	1418	43	1357	18	1306	16	96%	1418	43	Core
15G06-115	304	354	0.86	3.5040	0.1215	0.2762	0.0059	1421	61	1528	27	1572	30	97%	1421	61	Core
15G06-104	115	189	0.61	2.8150	0.0845	0.2219	0.0046	1456	50	1360	23	1292	24	94%	1456	50	Core
15G06-73	167	507	0.33	2.9272	0.0817	0.2262	0.0041	1484	48	1389	21	1314	22	94%	1484	48	Core
15G06-82	141	580	0.24	6.4469	0.1431	0.3689	0.0059	2040	33	2039	20	2024	28	99%	2040	33	Core
15G06-71	34	409	0.08	5.4863	0.1641	0.2989	0.0051	2116	53	1898	26	1686	25	~~88%~~			Core
15G06-22	41	50	0.83	7.5294	0.2921	0.3763	0.0096	2272	64	2176	35	2059	45	94%	2272	64	Core
15G06-56	185	168	1.10	7.6802	0.2358	0.3620	0.0076	2361	39	2194	28	1992	36	90%	2361	39	Core
15G06-52	316	463	0.68	7.4121	0.2026	0.3412	0.0058	2403	47	2162	25	1892	28	~~86%~~			Core
15G06-4	127	115	1.10	8.7465	0.2417	0.4038	0.0075	2405	46	2312	25	2187	34	94%	2405	46	Core
15G06-2	206	268	0.77	8.7735	0.2185	0.4023	0.0061	2417	40	2315	23	2180	28	93%	2417	40	Core
15G06-88	179	267	0.67	8.9335	0.1939	0.4081	0.0059	2418	35	2331	20	2206	27	94%	2418	35	Core
15G06-87	389	408	0.95	9.2311	0.2116	0.4211	0.0072	2420	32	2361	21	2265	33	95%	2420	32	Core
15G06-84	59	63	0.93	9.6509	0.2487	0.4448	0.0088	2422	38	2402	24	2372	39	98%	2422	38	Core
15G06-60	103	118	0.87	10.0963	0.2926	0.4551	0.0087	2450	44	2444	27	2418	39	98%	2450	44	Core
15G06-65	341	352	0.97	9.7782	0.2699	0.4305	0.0070	2454	48	2414	25	2308	32	95%	2454	48	Core
15G06-66	404	678	0.60	7.8432	0.2021	0.3453	0.0050	2457	47	2213	23	1912	24	~~85%~~			Core
15G06-45	35	36	0.96	8.8925	0.3471	0.4000	0.0091	2457	69	2327	36	2169	42	92%	2457	69	Core
15G06-95	115	88	1.31	9.1703	0.2089	0.4058	0.0057	2472	40	2355	21	2196	26	92%	2472	40	Core
15G06-31	364	420	0.87	11.5269	0.3935	0.4519	0.0098	2649	50	2567	32	2404	44	93%	2649	50	Core
15G44-5, Garnet-sillimanite gneiss																	
15G44-5-114	16	136	0.12	0.1997	0.0176	0.0286	0.0020	383	186	185	15	182	12	98%	182	12	Core
15G44-5-30	183	201	0.91	0.3657	0.0380	0.0438	0.0015	635	241	316	28	276	9	~~86%~~			Core
15G44-5-98	338	1577	0.21	0.4437	0.0185	0.0546	0.0018	554	74	373	13	343	11	91%	343	11	Core
15G44-5-36	106	1518	0.07	0.4499	0.0319	0.0603	0.0022	320	94	377	22	378	13	99%	378	13	Rim
15G44-5-29	100	1254	0.08	0.5433	0.0366	0.0612	0.0023	731	154	441	24	383	14	~~85%~~			Rim
15G44-5-119	79	1157	0.07	0.5398	0.0223	0.0641	0.0012	591	83	438	15	401	8	91%	401	8	Rim
15G44-5-68	574	920	0.62	0.5537	0.0428	0.0646	0.0019	611	123	447	28	404	12	~~89%~~			Core
15G44-5-56	483	376	1.28	0.5379	0.0627	0.0653	0.0016	554	251	437	41	408	10	93%	408	10	Core
15G44-5-46	247	233	1.06	0.5346	0.0271	0.0669	0.0021	520	111	435	18	418	12	95%	418	12	Core
15G44-5-40	9	606	0.01	0.5926	0.0479	0.0671	0.0032	717	149	473	31	419	19	~~87%~~			Rim
15G44-5-49	241	164	1.47	0.5625	0.0284	0.0681	0.0018	576	127	453	18	425	11	93%	425	11	Core
15G44-5-87	271	1405	0.19	0.6097	0.0161	0.0687	0.0015	739	46	483	10	428	9	~~87%~~			Core

Continued Table 3

Grain No.	Element (ppm)		Th/U	$^{207}Pb/^{235}U$	1σ	$^{206}Pb/^{238}U$	1σ	Age (Ma)						Concor	Used ages		Postion
	Th	U						$^{207}Pb/^{206}Pb$	1σ	$^{207}Pb/^{235}U$	1σ	$^{206}Pb/^{238}U$	1σ				
15G44-5-75	73	55	1.32	0.5957	0.0443	0.0697	0.0021	722	154	475	28	434	12	91%	434	12	Core
15G44-5-110	971	562	1.73	0.5283	0.0167	0.0698	0.0013	387	66	431	11	435	8	99%	435	8	Core
15G44-5-109	10	83	0.13	0.6445	0.0538	0.0703	0.0039	831	153	505	33	438	23	~~85%~~			Core
15G44-5-103	296	264	1.12	0.5474	0.0355	0.0719	0.0020	467	131	443	23	447	12	99%	447	12	Core
15G44-5-27	264	589	0.45	0.6387	0.0300	0.0724	0.0029	731	85	501	19	451	17	~~89%~~			Core
15G44-5-3	216	691	0.31	0.6358	0.0202	0.0725	0.0017	722	54	500	13	451	10	~~89%~~			Rim
15G44-5-96	254	555	0.46	0.6067	0.0178	0.0729	0.0015	617	59	481	11	454	9	94%	454	9	Core
15G44-5-107	476	376	1.26	0.6104	0.0219	0.0730	0.0024	676	79	484	14	454	14	93%	454	14	Core
15G44-5-63	150	119	1.26	0.6421	0.0390	0.0731	0.0027	665	113	504	24	455	16	~~89%~~			
15G44-5-16	535	533	1.00	0.5954	0.0173	0.0735	0.0011	543	63	474	11	457	6	96%	457	6	Rim
15G44-5-73	477	364	1.31	0.5818	0.0208	0.0738	0.0017	450	70	466	13	459	10	98%	459	10	Core
15G44-5-23	68	1304	0.05	0.5733	0.0176	0.0741	0.0013	428	72	460	11	461	8	99%	461	8	Rim
15G44-5-13	176	430	0.41	0.6691	0.0426	0.0748	0.0041	765	77	520	26	465	25	~~88%~~			
15G44-5-19	62	649	0.10	0.6799	0.0252	0.0752	0.0019	769	68	527	15	468	11	~~88%~~			
15G44-5-105	90	68	1.33	0.6013	0.0476	0.0755	0.0024	528	178	478	30	469	15	98%	469	15	Core
15G44-5-5	247	345	0.72	0.6224	0.0215	0.0761	0.0014	561	72	491	13	473	9	96%	473	9	Core
15G44-5-44	59	534	0.11	0.7305	0.0231	0.0784	0.0019	856	61	557	14	487	12	~~86%~~			
15G44-5-43	84	406	0.21	0.6499	0.0183	0.0784	0.0014	611	31	508	11	487	9	95%	487	9	Core
15G44-5-51	479	624	0.77	0.8727	0.0409	0.0975	0.0020	743	98	637	22	600	12	94%	600	12	Core
15G44-5-83	93	675	0.14	0.9009	0.0240	0.0991	0.0018	791	66	652	13	609	10	93%	609	10	Core
15G44-5-22	131	442	0.30	0.9546	0.0565	0.1007	0.0026	857	113	680	29	619	15	90%	619	15	Core
15G44-5-15	277	1118	0.25	0.9311	0.0242	0.1020	0.0019	792	60	668	13	626	11	93%	626	11	Core
15G44-5-62	66	103	0.64	0.8672	0.0403	0.1030	0.0021	561	98	634	22	632	12	99%	632	12	Core
15G44-5-41	177	1122	0.16	0.9689	0.0238	0.1032	0.0016	850	44	688	12	633	9	91%	633	9	Core
15G44-5-85	36	51	0.70	0.9832	0.0567	0.1039	0.0031	892	119	695	29	637	18	91%	637	18	Core
15G44-5-57	84	179	0.47	1.0397	0.0360	0.1046	0.0017	972	75	724	18	641	10	~~87%~~			
15G44-5-79	79	448	0.18	1.0115	0.0760	0.1046	0.0038	843	81	710	38	641	22	~~89%~~			
15G44-5-52	130	483	0.27	1.0432	0.0285	0.1051	0.0024	972	50	726	14	644	14	~~88%~~			
15G44-5-32	113	359	0.31	1.0058	0.0446	0.1052	0.0036	894	76	707	23	645	21	90%	645	21	Core
15G44-5-18	234	877	0.27	1.0354	0.0297	0.1053	0.0022	943	44	722	15	645	13	~~88%~~			
15G44-5-97	30	252	0.12	0.8786	0.0659	0.1054	0.0050	700	204	640	36	646	29	99%	646	29	Core
15G44-5-111	161	215	0.75	1.0376	0.0441	0.1056	0.0033	943	77	723	22	647	19	~~89%~~			
15G44-5-84	19	549	0.04	1.0245	0.0324	0.1069	0.0024	900	52	716	16	655	14	91%	655	14	Core
15G44-5-82	154	308	0.50	1.0123	0.0341	0.1070	0.0023	865	137	710	17	655	13	91%	655	13	Core
15G44-5-118	60	58	1.04	1.0270	0.0590	0.1072	0.0028	909	117	717	30	657	17	91%	657	17	Core
15G44-5-14	251	272	0.92	1.0468	0.0391	0.1077	0.0023	924	69	727	19	660	13	90%	660	13	Core
15G44-5-42	559	703	0.79	0.9552	0.0224	0.1086	0.0017	715	14	681	12	665	10	97%	665	10	Core
15G44-5-117	248	583	0.43	1.0745	0.0311	0.1088	0.0023	939	53	741	15	666	13	~~89%~~			
15G44-5-71	87	95	0.91	1.1087	0.0432	0.1202	0.0030	833	81	758	21	732	17	96%	732	17	Core
15G44-5-65	941	831	1.13	1.2000	0.0366	0.1218	0.0024	900	56	801	17	741	14	92%	741	14	Core
15G44-5-11	42	862	0.05	1.2250	0.0593	0.1231	0.0045	959	71	812	27	748	26	91%	748	26	Core
15G44-5-48	622	1522	0.41	1.1578	0.0214	0.1237	0.0016	856	35	781	10	752	9	96%	752	9	Core
15G44-5-53	143	451	0.32	1.1854	0.0330	0.1244	0.0020	878	52	794	15	756	11	95%	756	11	Core
15G44-5-6	17	631	0.03	1.2483	0.0347	0.1254	0.0027	969	44	823	16	762	15	92%	762	15	Core
15G44-5-99.2	103	170	0.60	1.2545	0.0467	0.1258	0.0033	989	58	825	21	764	19	92%	764	19	Core
15G44-5-59	123	522	0.24	1.2699	0.0392	0.1266	0.0027	972	53	832	18	768	16	92%	768	16	Core
15G44-5-7	47	77	0.61	1.1500	0.0575	0.1266	0.0036	843	115	777	27	769	20	98%	769	20	Core
15G44-5-77	102	259	0.39	1.1897	0.0385	0.1270	0.0020	828	66	796	18	771	12	96%	771	12	Core
15G44-5-10	83	164	0.51	1.2715	0.0835	0.1273	0.0046	967	99	833	37	772	26	92%	772	26	Core
15G44-5-58	90	433	0.21	1.3104	0.0426	0.1302	0.0027	989	61	850	19	789	15	92%	789	15	Core
15G44-5-12	18	483	0.04	1.4320	0.0485	0.1318	0.0037	1150	84	902	20	798	21	~~87%~~			
15G44-5-26	28	120	0.23	1.3755	0.0493	0.1361	0.0025	1000	78	879	21	822	14	93%	822	14	Core
15G44-5-99	29	750	0.04	1.4059	0.0344	0.1365	0.0022	1039	38	891	15	825	12	92%	825	12	Core
15G44-5-89	263	676	0.39	1.3258	0.0274	0.1375	0.0022	917	40	857	12	831	12	96%	831	12	Core
15G44-5-90	170	248	0.69	1.3475	0.0359	0.1387	0.0026	940	44	866	16	837	15	96%	837	15	Core
15G44-5-25	975	603	1.62	1.3601	0.0350	0.1391	0.0022	920	45	872	15	840	12	96%	840	12	Core
15G44-5-66	164	227	0.72	1.3635	0.0371	0.1392	0.0023	909	56	873	16	840	13	96%	840	13	Core
15G44-5-113	380	968	0.39	1.3510	0.0318	0.1396	0.0023	902	43	868	14	842	13	96%	842	13	Core
15G44-5-95	272	602	0.45	1.3594	0.0283	0.1397	0.0018	1000	39	872	12	843	10	96%	843	10	Core
15G44-5-60	404	424	0.95	1.3951	0.0390	0.1398	0.0021	969	59	887	17	843	12	94%	843	12	Core
15G44-5-88	74	167	0.44	1.4253	0.0399	0.1415	0.0023	1017	55	900	17	853	13	94%	853	13	Core
15G44-5-93	160	444	0.36	1.3466	0.0335	0.1420	0.0020	889	50	866	15	856	12	98%	856	12	Core
15G44-5-35	1527	924	1.65	1.4376	0.0405	0.1424	0.0032	989	41	905	17	858	18	94%	858	18	Core
15G44-5-70	156	143	1.09	1.3871	0.0437	0.1426	0.0027	902	69	883	19	859	15	97%	859	15	Core
15G44-5-86	253	180	1.40	1.4230	0.0494	0.1444	0.0035	946	63	899	21	870	20	96%	870	20	Core
15G44-5-94	155	446	0.35	1.6846	0.0444	0.1524	0.0048	1221	81	1003	17	914	27	90%	914	27	Core
15G44-5-24	1017	815	1.25	2.3673	0.0710	0.1992	0.0044	1321	48	1233	21	1171	24	94%	1321	48	Core
15G44-5-92	330	518	0.64	3.3614	0.0861	0.2213	0.0045	1794	46	1495	20	1289	24	~~85%~~			
15G44-5-100	134	249	0.54	4.6483	0.2187	0.2939	0.0085	1857	67	1758	39	1661	42	94%	1857	67	Core
15G44-5-8	46	1171	0.04	5.7135	0.1581	0.3125	0.0058	2113	50	1933	24	1753	29	90%	2113	50	Core
15G44-5-37	311	786	0.40	8.1008	0.2405	0.4055	0.0062	2257	38	2242	27	2194	29	97%	2257	38	Core
15G44-5-91	238	534	0.45	10.0637	0.2300	0.4080	0.0070	2640	36	2441	21	2206	32	~~89%~~			Core
15G44-5-104	37	79	0.47	16.3316	0.5744	0.5205	0.0098	3031	54	2896	34	2701	42	93%	3031	54	Core
15G44-5-47	271	675	0.40	23.9190	0.7056	0.5745	0.0169	3461	33	3265	29	2926	69	~~89%~~			Core

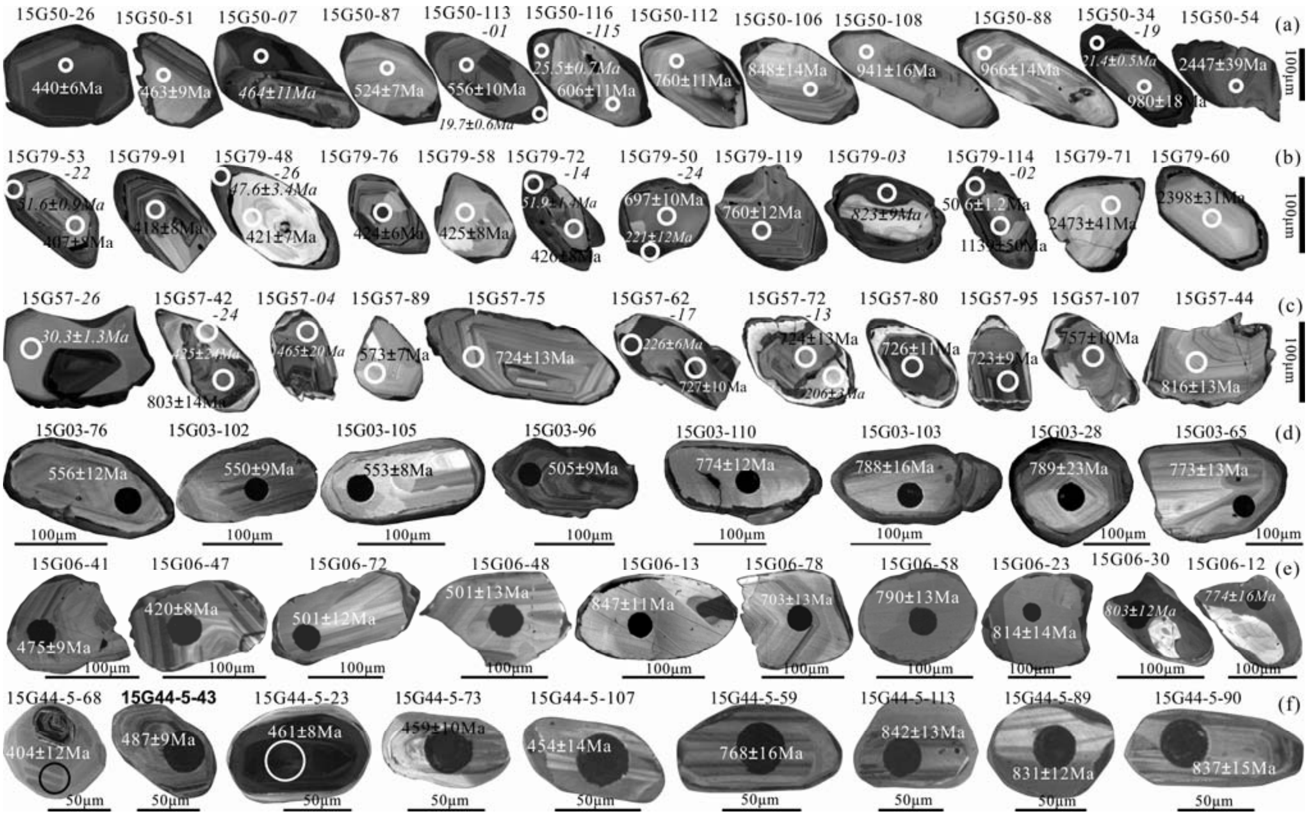

Fig. 5. Cathodoluminescence (CL) images showing internal structures of representative zircons. The results are marked using a circle (25 μm) with ages.

in length, and most of them are sub-rounded to sub-angular in shape with aspect ratios from 1:1 to 2:1. The internal textures of most zircons revealed by CL images contain concentric zoning, sector zoning, or banded zoning and a 10-50 mm homogeneous and low-fluorescence overgrowth rim (Fig. 5a). A total of 117 spots were analysed from 101 zircon grains for this sample, including 87 detrital zircon cores and 30 overgrowth rims. Correspondingly, two significant age groups were identified from the distinct zircon domains. Nineteen out of the 30 analysed spots on the overgrowth rims yielded concordant ages from 19.5±0.5 Ma to 35.0±1.0 Ma (Fig. 6a) and low Th/U ratios (0.02–0.12). In contrast, 98 analysed spots yielded concordant ages ranging from 440±6 Ma to 3569±30 Ma, with three major peaks at 480 Ma, 955 Ma and 2480 Ma (Fig. 7a), and 86 of the 87 analysed spots in the oscillatory cores had high Th/U ratios (0.15 to 2.91).

4.2.2 Sample 15G79

The zircon grains from the sample 15G79 are 100-200 mm in length and have aspect ratios ranging from 1:1 to 2.5:1 (Fig. 5b). The CL images reveal that most of the zircon grains show distinct concentric oscillation, indicating a large proportion of igneous zircons. A small portion possesses metamorphic characteristics, including a sub-rounded morphology and a homogeneous metamict internal structure. In total, 120 spots, including 90 magmatic cores and 30 overgrowth rims, were analysed on 103 zircon grains from sample 15G79, and the data from 115 spots with discordances less than 10% were taken for statistical interpretation. Among these spots, 94 spots in the inherited (magmatic) zircon cores yielded concordant ages ranging from 396±7 Ma to 3068±38 Ma (Fig. 6b). In addition to a late Archean peak (2450 Ma) and a Neoproterozoic peak (876 Ma), the youngest peak is at 424 Ma with a cluster of 19 zircons (Fig. 7b). Most of these analysed spots (except five spots) were characterized by high Th/U ratios (>0.1). Two significant age groups were identified in the overgrowth rims from this two-mica schist. For the first group, 16 spots yielded $^{206}Pb/^{238}U$ ages of 47.1±1.1 Ma to 59.9±1.3 Ma (two older ages of 65.0 Ma and 77.8 Ma were eliminated) and low Th/U ratios (<0.02). For the second group, three spots in overgrowth rims yielded $^{206}Pb/^{238}U$ ages of 221±12 Ma to 239±19 Ma and Th/U ratios of 0.02–0.16.

4.2.3 Sample 15G57

The zircon grains from the garnet-bearing two-mica schist (15G57) are variable in size (80–250 mm in length) and mostly sub-angular to sub-rounded in shape with length/width ratios of approximately 1:1−3:1. The CL analysis showed cores with concentric zoning or banded zoning, and most of the zircons possessed 5–50 mm overgrowth rims with variable (white, grey and black) luminescence (Fig. 5c). In total, one hundred and twenty spots were measured on 113 grains from this sample, and the results can be divided into three significant age groups. All inherited (detrital) cores have high Th/U ratios (0.11–1.66), and 96 analysed spots yield concordant U-Pb ages

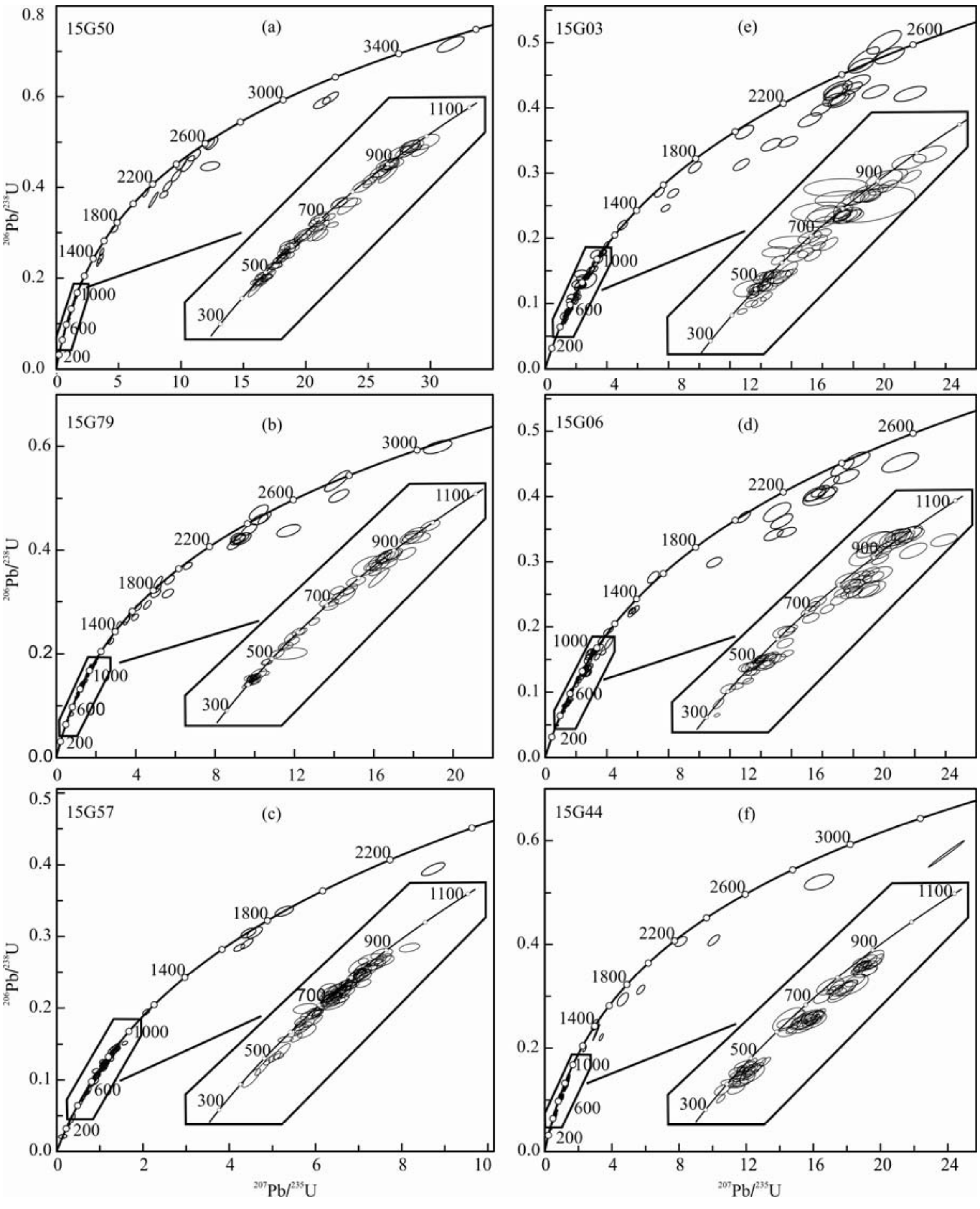

Fig. 6. U-Pb concordia diagrams of detrital zircon analyses from the ALS Group, southwestern South China Block. Inserted diagrams show the representative ranges of the analysed samples.

ranging from 425±24 to 2457±24 Ma (Fig. 6c) with a major peak at 732 Ma in the probability density diagram (Fig. 7c). No Palaeozoic age peak is present in this sample. Moreover, the two youngest inherited ages were observed in the rims of two zircons. Moreover, the metamorphic overgrowth zircon domains are characterized by variable Th/U ratios (0.01–1.01) and can be subdivided into two groups. The eight analysed spots of the first group yield $^{206}Pb/^{238}U$ ages ranging from 23.1±0.6 Ma to 38.1±1.5 Ma, and the 13 analysed spots of the second group yield $^{206}Pb/^{238}U$ ages between 128±2 Ma and 285±30 Ma.

4.2.4 Sample 15G03

The zircons from the garnet-sillimanite gneiss sample (15G03) are relatively short (80–180 mm) and have low

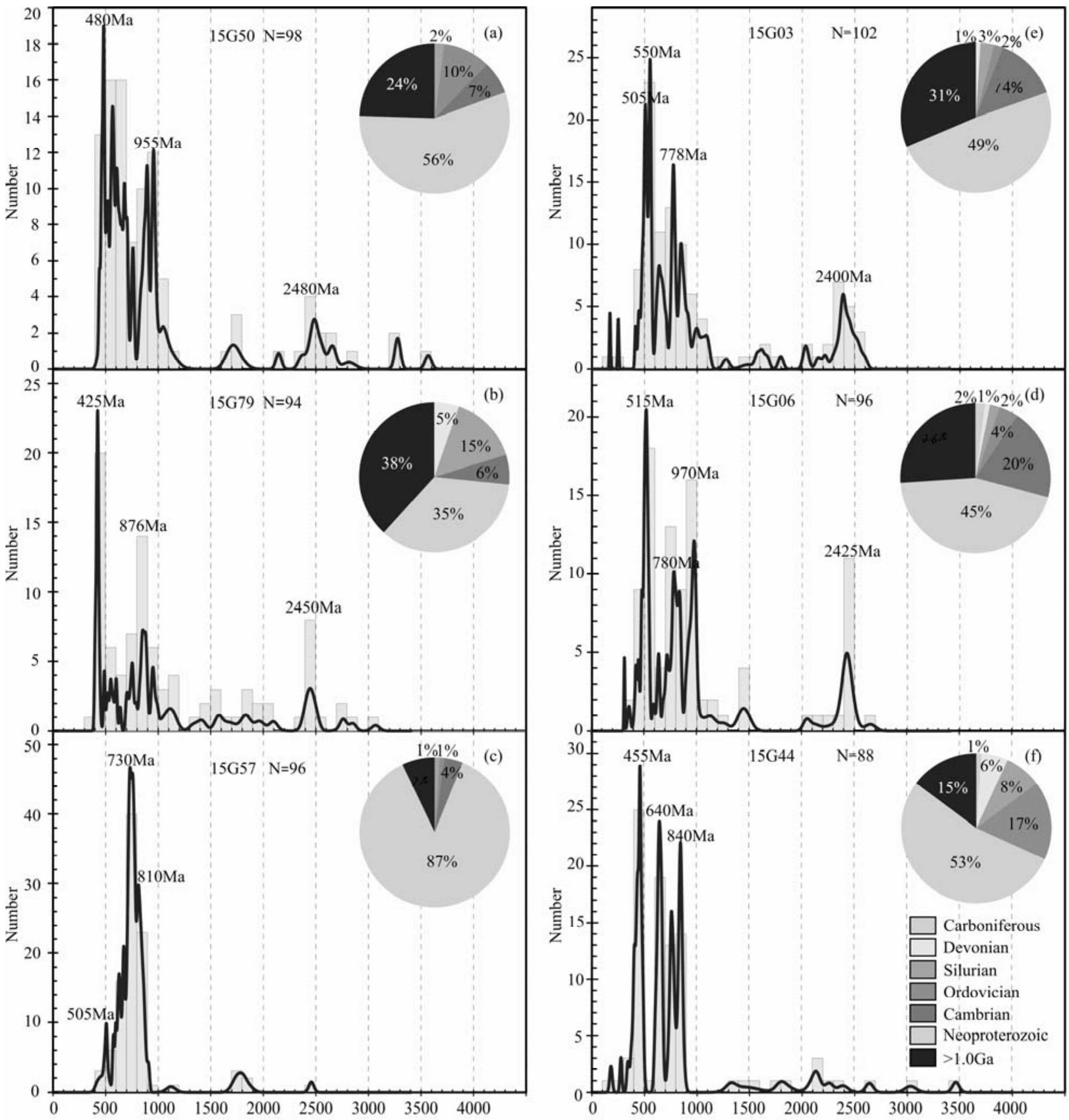

Fig. 7. Relative probability plots and age distribution histograms with bin widths of 40 m.y. showing ages of detrital zircons from lithic and basaltic sandstones. $^{206}Pb/^{238}U$ ages are given for zircons younger than 1000 Ma, and $^{207}Pb/^{206}Pb$ ages are given for those that are 1000 Ma or older.

aspect ratios from 1:1 to 2:1. The CL images exhibit internal textures of concentric zoning, patchy zoning and banded zoning, and around the core, most zircon grains possessed a narrow (5–20 mm) overgrowth rim (Fig. 5d). The 117 inherited (detrital) cores yield 103 concordant ages (with discordances less than 15%) that range from 171±5 Ma to 2839±45 Ma (Fig. 6d). The most significant age cluster, constituting 30% of the analysed grains, lies between 415 Ma and 564 Ma and has an age peak at 508-550 Ma (Fig. 7d). Subordinate age peaks exist at 778 Ma and 2400 Ma. The youngest cluster comprises 31 ages (415–564 Ma). Additionally, except for four analysed spots, all inherited cores exhibit high Th/U ratios (>0.1).

4.2.5 Sample 15G06

The zircon grains from sample 15G06 are 120–200 mm in length, and most of them are sub-rounded or oval in shape, with aspect ratios of 1:1 to 2:1. The internal textures revealed by CL images include concentric zoning, sector zoning and banded zoning in the low-luminescence inherited cores, and the cores are surrounded by narrow overgrowth rims (Fig. 5e). One hundred and five zircon grains were measured for sample 15G06, and 96 U-Pb ages with discordances less than 15% are considered statistically (Fig. 6e). Most of these zircon spots have high Th/U ratios (>0.1), and only four analysed spots were excluded. The data define four dominant age populations at 440-550 Ma, 740–840 Ma, 940–1140 Ma and 2400–2480 Ma. In the probability diagram (Fig. 7e), clear age peaks are observed at 516 Ma, 782 Ma, 970 Ma, and 2425 Ma. The youngest peak consists of 24 spots and constitutes 30% of the analysed grains.

4.2.6 Sample 15G44

The zircons separated from sample 15G44 are mainly rounded, equidimensional, or oval in shape and have lengths of 70 to 150 μm, with aspect ratios of ~1:1 to 2:1. In CL images, most grains display 5–10 mm overgrowth rims around highly luminescent cores, and most of the cores display clear oscillatory zones (Fig. 5f). We analysed 116 grains and considered the data from 86 spots with discordance less than 15% acceptable for statistical analysis (Fig. 6f). Seventy-five of the 86 spots show high Th/U ratios ranging from 0.10 to 1.73. The grains with oscillatory or irregular zoning form groups with dominantly early Palaeozoic (418–487 Ma) and Neoproterozoic (600–914 Ma) ages, and these two age groups constitute 81% of the total analysed grains. The probability density diagram shows three dominant age peaks at 456 Ma, 640 Ma and 842 Ma (Fig. 7f). The youngest peak in the early Palaeozoic consists of 25 ages and comprises 29% of the total number of ages.

5 Discussion

5.1 Ages of deposition and metamorphism

In the last two decades, geochronological studies in both the SCB and Indochina Block have investigated many high-grade metamorphic complexes/massifs traditionally considered to be Archean or Palaeoproterozoic in age. These studies have demonstrated that the protoliths of the metasedimentary rocks in some of these metamorphic complexes, such as the Kontum massif (Usuki et al., 2009; Burret et al., 2014) and Lancang complex (Nie et al., 2015; Xing et al., 2016) in Indochina Block and Kangding complex (Zhou et al., 2002) and Wugong and Wuyi-Yunkai domains (Wang et al., 2011) in the SCB, were deposited during the Neoproterozoic-early Palaeozoic. Some researchers have proposed that the ALS metamorphic belt is a complex composed of multiple rock types from different periods. However, due to high-grade metamorphism and multistage tectonic superposition, published inherited zircon ages from sedimentary rocks in the ALS Group are rare. These rocks have traditionally been interpreted to be Palaeoproterozoic in age (BGMRY, 1990), but the depositional ages of the ALS Group have not been well defined. Zhai et al. (1990) obtained a Sm-Nd isochron age of 1367.1±46.1 Ma for amphibolite and an $^{40}Ar/^{39}Ar$ age of 1710.3±2.4 Ma for garnet pyroxenite and interpreted them as a Mesoproterozoic metamorphic age and the depositional age of the ALS Group, respectively. Thus, those authors concluded that the ALS Group was deposited in the Palaeoproterozoic. Due to the overprinting of multiple tectonothermal events and the constraints imposed by geographical conditions, very little data on detrital zircon ages in the ALS Group have been published, despite being the largest complex (more than 5000 km^2) in the southeastern Tibetan Plateau. Wang et al. (2013) once reported 92 spot analyses on the detrital zircon cores from one quartzite from the ALS Group in the Yuanyang area. The zircon grains yielded two major age populations at 493–528 Ma (n=42) and 701-784 Ma (n=44). Liu F L et al. (2013) also reported relative probability plots for inherited zircon ages (n=184) from a paragneiss and a marble in the ALS Group, which also yielded a youngest peak at 515 Ma. Ji Lei et al. (2018) reported detrital zircon ages for one dolomitic marble and two metapelites from the eastern part of the ALS Group (Along Formation), and these units exhibited minimum age peaks at 452 Ma, 461 Ma and 458-505 Ma, respectively. However, all previously analysed samples were collected from the eastern part of the ALS Group (Along Formation), and the ages of other formations remain unclear. In this paper, six metasedimentary rocks were collected from the ALS Group (including both the Xiaoyangjie and Along formations) along the southwest margin of the SCB. Except for sample 15G57, which shows a single Neoproterozoic peak (732 Ma), the youngest peaks in the five other samples correspond to the early Palaeozoic (480 Ma, 424 Ma, 508–550 Ma, 516 Ma, 456 Ma) and account for more than 20% of the total grains. It should be mentioned that all these ages were obtained from inherited magmatic zircon cores and with high Th/U ratio (>0.1) rather than the metamorphic overgrowth rims. Therefore, we suggest that the youngest population of 424-516 Ma represents the maximum depositional age of the ALS Group. The difference in the maximum depositional age and age pattern between these samples may be interpreted as different depositional ages and/or different sedimentary sources (Cawood et al., 2012). The detrital age distribution of the samples 15G03, 15G06 and 15G50 from the ALS Group lack information of 460–420 Ma, and the minimum peaks are 505 Ma, 515 Ma, 480 Ma, respectively, which possibly indicates that protoliths for these samples were deposited during Cambrian to Ordovician. Samples 15G79 and 15G44 show peaks corresponding to the Silurian (425 Ma) and late Ordovician (455 Ma), and Devonian ages account for 5% and 6% in these two samples, respectively. Furthermore, ages younger than the Devonian are absent from both samples, which indicates that they may have been deposited during the Devonian to Carboniferous. Sample 15G57 contains a single peak at 730 Ma, which may be interpreted as the derivation of material from the middle Neoproterozoic plutons in the northern and western SCB.

Notably, the Permo-Triassic metamorphic event (270–210 Ma) is pervasive throughout the ALS belt and its southern extension known as the Day Nui Con Voi Complex, as well as in the adjacent regions in both the SCB and Indochina Block (Gilley et al., 2003; Liu et al., 2013; Zelazniewicz et al., 2013; Faure et al., 2018;

Nakano et al., 2018). Therefore, the metasedimentary rocks in the ALS Group are older than the middle Permian. Additionally, our geochronological data indicate that two samples (15G79 and 15G57) record Indosinian metamorphic events and that three samples (15G79, 15G50 and 15G57) record the most prevalent Eocene metamorphic age in the ALS belt.

The synthesis of all data suggests that the protolith age of major sedimentary rocks in the ALS Group is Palaeozoic and may be equivalent to the Cambrian-Carboniferous strata in the low-grade metamorphic unit of the ALS belt rather than the traditionally considered Palaeoproterozoic basement of the SCB. Some of middle-late Neoproterozoic granitic gneisses in the ALS belt may have been the provenance of the ALS Group and should be removed from the ALS Group. Tectonothermal overprinting occurred during the Permo-Triassic due to the collision between the Indochina Block and the SCB and during Cenozoic due to the India-Asia collision. Furthermore, the crustal-scale ALS-RR strike-slip shearing was also documented after diagenesis of these sedimentary rocks.

5.2 Depositional setting of the ALS Group

Many tectonic discrimination diagrams have been built to infer the provenance of sedimentary rocks (Bhatia 1983; Bhatia and Crook, 1986; Roser and Korsch, 1986); however, due to the high mobility of specific oxides and elements during weathering and transport processes, most of these diagrams have low success rates (less than 30%) and do not perform satisfactorily (Armstrong-Altrin and Verma, 2005; Weltje, 2006; Ryan and Williams, 2007; Verma and Armstrong-Altrin, 2016). Trace elements, such as REEs, Zr, Nb, Ti, Th, Sc, and Ni, exhibit relatively low mobility and are more resistant during weathering and transport, and their elemental ratios have been proven to be most useful for inferring sediment provenance (Bhatia and Crook, 1986; Cullers, 2000, 2002). These elements are used for sedimentary source discrimination in this study (Fig. 8a–d)

The Th/U ratios of sedimentary rocks are expected to increase with increasing weathering and recycling due to the oxidation and loss of uranium (McLennan et al., 1990, 1993). In the Zr/Sc-Th/Sc plot, all samples, except for 15G74, cluster roughly around the trend defined by different source rocks, indicating that zircon addition did not occur during the deposition of the ALS Group and overlying sequences (Fig. 8a).

Floyd and Leveridge (1987) established a discrimination diagram using the La/Th ratio vs. Hf content to determine sediment sources. High La/Th ratios and low Hf contents suggest derivation dominantly from a

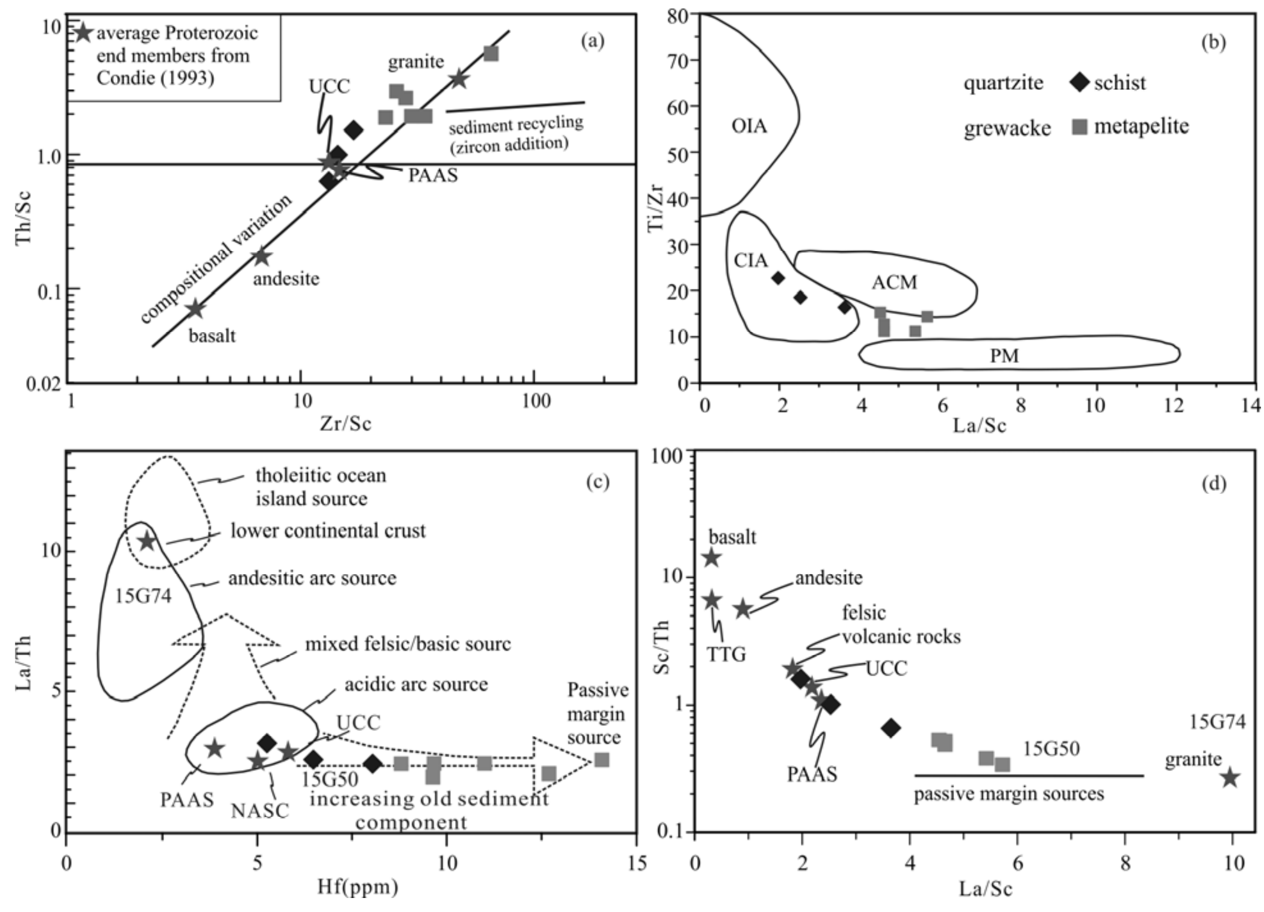

Fig. 8. Source rock discrimination diagrams illustrating sedimentary provenance.

(a) Th/Sc vs. Zr/Sc diagram (after McLennan et al., 1993). (b) La/Sc vs. Ti/Zr (after Bhatia and Crook, 1986). (c) La/Th vs. Hf diagram after Floyd and Leveridge (1987). (d) Sc/Th vs. La/Sc diagram (after Wang et al., 2018). OIA = oceanic island arc; CIA = continental island arc; ACM = active continental margin; PM= passive margin. PAAS and UCC values are from Taylor and McLennan (1985), and the NASC value is from Condie (1993).

mafic arc source. On the La/Th vs. Hf diagram (Fig. 8c), most samples (La/Th=4.9–16.8 ppm, Hf=4.53–14.1 ppm) plot in the acidic arc and passive margin source fields, suggesting derivation from acidic arc rocks with some proportion of old recycled sediments.

On the La/Sc-Ti/Zr, La/Th-Hf and La/Sc-Sc/Th tectonic discrimination plots, most of the samples exhibit the characteristics of an acidic arc source or passive continental margin source and contain some proportion of old sediments (Fig. 8b–d). These features are similar to those of post-Archean average Australian shale (PAAS) and North American shale composite (NASC) (Condie, 1993). Thus, we conclude that the two major sources of the ALS Group are felsic volcanic rocks and old recycled sediments. Palaeogeographic reconstruction of South China revealed that during earliest early paleozoic exist an old land in western SCB (Wang et al., 2012) and the ripple mark and flute cast in early paleozoic sediments indicate the paleocurrent was from SE to NW (Wang et al., 2010). Therefore, the most likely provenance might be the widespread early Palaeozoic magmatic plutons and strata that formed during the Kwangsian Orogeny in the Cathaysia Block (Wang et al., 2010, 2011); another early Palaeozoic material source for the ALS Group may be the Ordovician-Silurian volcanic rocks on the western margin of the Indochina Block (Nie et al., 2015; Mao et al., 2017), which are related to blocks that separated from eastern Gondwana. The Panxi-Hannan-Ailaoshan arc on the northwestern and southwestern margin of the SCB (Wang et al., 2016, 2017) might have provided Neoproterozoic detritus to the ALS Group.

6 Conclusion

This study reports a new set of geochemical data and in situ zircon U-Pb ages of detrital zircons from metasedimentary rocks from the ALS Group in the southwestern SCB. Our LA-ICP-MS U-Pb ages provide new insights into the tectonic-magmatic evolution of the southwest margin of SCB during the Palaeozoic. Through compilation of detrital zircon age distributions of samples from other terranes in SE Asia, we have reached the following conclusions.

(1) U-Pb analysis of detrital zircons from the ALS Group reveals two major age peaks at ca. 510 Ma and 760 Ma, along with three subordinate age peaks at ca. 840 Ma, 960 Ma and 2450 Ma. The ALS Group is mainly composed of Palaeozoic (Cambrian-Carboniferous) sedimentary rocks rather than Palaeoproterozoic basement of the SCB as previously studies.

(2) The ALS Group received detritus derived from intermediate and felsic igneous rocks that formed in a continental arc setting and from recycled metasedimentary strata. After deposition, the ALS Group experienced two tectonothermal events in the Indonesian and Cenozoic.

(3) The ALS Group might be derived from the magmatic plutons and strata that formed during the Kwangsian Orogeny in the Cathaysia Block, the Ordovician-Silurian volcanic rocks on the western margin of the Indochina Block and the arc-related Neoproterozoic magmatic rocks on the northwestern and southwestern margin of the SCB.

Acknowledgements

The research was supported by the National Natural Science Foundation of China (Project No. 91855206, 41802072 and 41372069), the national key research and development plan (Project No. 2016YFC0600310), and China Postdoctoral Science Foundation (Project No. 2017M620853). We thank Profs. Qunke Xia and Chaohui Liu for their constructive comments.

Manuscript received Feb. 25, 2019
accepted Apr. 8, 2019
associate EIC FEI Hongcai
edited by FEI Hongcai

References

Armstrong-Altrin, J.S., and Verma, S.P., 2005. Critical evaluation of six tectonic setting discrimination diagrams using geochemical data of Neogene sediments fromknown tectonic settings. Sedimentary Geology, 177: 115–129.

Bhatia, M.R., and Crook, A.W., 1986. Trace element characteristics of graywackes and tectonic setting discrimination of sedimentary basins. Contributions to Mineralogy and Petrology, 92: 181–193.

Bhatia, M.R., 1983. Plate tectonics and geochemical composition of sandstones. Journal of Geology, 91(6): 611–627.

BGMRY (Bureau of Geology and Mineral Resources of Yunnan Province), 1990. Regional Geology of Yunnan Province. Beijing: Geological Publishing House, 1–728 (in Chinese with English abstract).

Cai, Y.F., Wang, Y.J., Cawood, P.A., Fan, W.M., Liu, H.C., Xing, X.W., and Zhang, Y.Z., 2014. Neoproterozoic subduction along the Ailaoshan zone, South China: Geochronological and geochemical evidence from amphibolite. Precambrian Research, 245(5): 13–28.

Cai, Y.F., Wang, Y.j., Cawood, P.A., Zhang, Y.Z., and Zhang, A.M., 2015. Neoproterozoic crustal growth of the Southern Yangtze Block: Geochemical and zircon U–Pb geochronological and Lu-Hf isotopic evidence of Neoproterozoic diorite from the Ailaoshan zone. Precambrian Research, 266: 137–149.

Cawood, P.A., Hawkesworth, C.J., and Dhuime, B., 2012. Detrital zircon record and tectonic setting. Geology, 40: 875–878.

Chen, B.W., Li, Y.S., Qu, J.C., Wang, K.Y., Ai, C.G., and Zhu, Z.Z., 1991. On the main geotectonic problems in the Sanjiang region (Nujiang-Lancangjiang-Jinshajiang) and their relationship with mineralization. Beijing: Geological Publishing House, 1–110 (in Chinese with English abstract).

Chen, Q., Sun, M., Long, X.P., Zhao, G.C., and Yuan, C., 2016. U–Pb ages and Hf isotopic record of zircons from the late Neoproterozoic and Silurian–Devonian sedimentary rocks of the western Yangtze Block: Implications for its tectonic evolution and continental affinity. Gondwana Research, 31: 184–199.

Chen, Q., Sun, M., Long, X.P., Zhao, G.C., Wang, J., Yu, Y., and Yuan, C., 2018. Provenance study for the Paleozoic sedimentary rocks from the west Yangtze Block: Constraint on possible link of South China to the Gondwana supercontinent reconstruction. Precambrian Research, 309: 271–289.

Chen, X.Y., Liu, J.L., Fan, W.K., Qi, Y.C., Wang, W., Chen, Jiafu., and Burg, J.P., 2017. Neoproterozoic granitoids along the Ailaoshan-Red River belt: Zircon U-Pb geochronology, Hf isotope analysis and tectonic implications. Precambrian Research, 299: 244–263.

Condie, K.C., 1993. Chemical composition and evolution of the upper continentalcrust: contrasting results from surface samples and shales. Chemical Geology, 104(1–4): 1–37.

Cox, R., Lowe, D.R., and Cullers, R., 1995. The influence of sediment recycling and basement composition on evolution of mudrock chemistry in the southwestern United States. Geochimica et Cosmochimica Acta, 59(14): 2919–2940.

Cullers, R.L., 2000. The geochemistry of shales, siltstones and sandstones of Pennsylvanian–Permian age, Colorado, U.S.A.: implications for provenance and metamorphic studies. Lithos, 51(3): 181–203.

Cullers, R.L., 2002. Implications of elemental concentrations for provenance, redox conditions, and metamorphic studies of shales and limestones near Pueblo, CO, USA. Chemical Geology, 191(4): 305–327.

Deng, J., Wang, Q.F., Li, G.J., Li, C.S., and Wang, C.M., 2014. Tethys tectonic evolution and its bearing on the distribution of important mineral deposits in the Sanjiang region, SW China. Gondwana Research, 26(2): 419–437.

Fan, WM., Wang, Y.J., Zhang, A.M., Zhang, F.F., and Zhang, Y.Z., 2010. Permian arc–back-arc basin development along the Ailaoshan tectoniczone: Geochemical, isotopic and geochronological evidence fromthe Mojiang volcanic rocks, Southwest China. Lithos, 119(3): 553–568.

Faure, M., Lin, W., Chu, Y., and Lepvrier, C., 2016. Triassic tectonics of the Ailaoshan Belt (SW China): Early Triassic collision between the South China and Indochina Blocks, and Middle Triassic intracontinental shearing. Tectonophysics, 683: 27–42.

Faure, M., Nguyen, V.V., Hoai, L.T.T., and Lepvrier, C., 2018. Early Paleozoic or Early-Middle Triassic collision between the South China and Indochina Blocks: The controversy resolved? Structural insights from the Kon Tum massif (Central Vietnam). Journal of Asian Earth Sciences, 166: 162–180.

Fedo, C.M., Sircombe, K.N., and Rainbird, R.H., 2003. Detrital zircon analysis of the sedimentary record. Reviews in Mineralogy & Geochemistry, 53(1): 277–303.

Fedo, C.M., Wayne Nesbitt, H., and Young, G.M., 1995. Unraveling the effects of potassium metasomatism in sedimentary rocks and paleosols, with implications for paleoweathering conditions and provenance. Geology, 23(10): 921–924.

Floyd, P.A., and Leveridge, B.E., 1987. Tectonic environment of the Devonian Gramscathobasin, south Cornwall: framework mode and geochemical evidence from tur-biditic sandstones. Journal of the Geological Society of London, 144(4): 531–542.

Floyd, P.A., Shail, R., Leveridge, B.E., Franke, W., 1991. Geochemistry and provenance of Rhenohercynian synorogenic sandstones: implications for tectonic environment discrimination. Geological Society of London, Special Publication, 57(1): 173–188.

Gilley, L.D., Harrison, T.M., Leloup, P.H., Ryerson, F.J., Lovera, O.M., and Wang, J.H., 2003. Direct dating of left-lateral deformation along the Red River shear zone, China, Vietnam. Journal Geophysical Research Solid Earth, 108(B2): 2127. doi.org/10.1029/2001JB0011726.

Greentree, M.R., and Li, Zhengxiang., 2008. The oldest known rocks in south–western China: SHRIMP U–Pb magmatic crystallisation age and detrital provenance analysis of the Paleoproterozoic Dahongshan Group. Journal of Asian Earth Sciences, 33(5–6): 289–302.

Jackson, S.E., Pearson, N.J., Griffin, W.L., and Belousova, E.A., 2004. The application of laser ablation-inductively coupled plasma-mass spectrometry to in situ U–Pb zircon geochronology. Chemical Geology, 211(1–2): 49–69.

Ji, L., Liu, F.L., Wang, F., and Sun, Z.B., 2018. LA-ICP-MS U-Pb geochronology of detrital zircons from meta-sedimentary rocks within the Ailaoshan Group, western Yunnan. Acta Petrologica Sinica, 34(5): 1503–1516.

Lai, C.K., Meffre, S., Crawford, A.J., Zaw, K., Xue, C.D., and Halpin, J.A., 2014. The Western Ailaoshan Volcanic Belts and their SE Asia connection: a new tectonic model for the Eastern Indochina Block. Gondwana Research, 26(1): 52–74.

Liu, F.L., Wang, F., Liu, P.H., and Liu, C.H., 2013. Multiple metamorphic events revealed by zircons from the Diancang Shan−Ailaoshan metamorphic complex, southeastern Tibetan Plateau. Gondwana Research, 24(1): 429–450.

Liu, F.L., Wang, F., Liu, P.H., Yang, H., and Meng, E., 2015. Multiple partial melting events in the Ailaoshan–Red River and Gaoligong shan complex belts, SE Tibetan Plateau: zircon U–Pb dating of granitic leucosomes within migmatites. Journal of Asian Earth Sciences, 110: 151–169.

Liu, H.C., Wang, Y.J., Fan, W.M., Zi, J.W., Cai, Y.F., and Xing, X.W., 2014. Petrogenesis and tectonic implications of Late-Triassic high εNd(t)-εHf(t) granites in the Ailaoshan tectonic zone (SW China). Science China Earth Sciences, 57(9): 2181–2194.

Liu, J.L., Chen, X.Y., Wu, WB., Tang, Y., Tran, M.D., Nguyen, Q.L., Zhang, Z.C., and Zhao, Z.D., 2015. New tectono-geochronological constraints on timing of shearing along the Ailaoshan-Red River shear zone: Implications for genesis of Ailaoshan gold mineralization. Journal of Asian Earth Sciences, 103: 70–86.

Liu, J.L., Tang, Y., Tran, M.D., Cao, S.Y., Zhao, L., Zhang, Z.C., Zhao, Z.D., and Chen, W., 2012. The nature of the Ailaoshan–Red River (ASRR) shear zone: Constraints from structural, microstructural and fabric analyses of metamorphic rocks from the Diancang Shan, Ailaoshan and Day Nui Con Voi massifs. Journal of Asian Earth Sciences, 47(1): 231–251.

Liu, P.P., Zhou, M.F., Zhao, G.C., Chung, S.L., Chen, W.T., and Wang, F., 2017. Eocene granulite-facies metamorphism prior to deformation of the Mianhuadi mafic complex the Ailaoshan -Red River shear zone, Yunnan Province, SW China. Journal of Asian Earth Sciences, 145: 626–640.

Liu, Y.S., Hu, Z.C., Gao, S., Günther, D., Xu, J., Gao, C.G., and Chen, H.H., 2008. In situ analysis of major and trace elements of anhydrous minerals by LA-ICP-MS without applying an internal standard. Chemical Geology, 257(1): 34–43.

Ludwig, K.R., 2003. ISOPLOT 3.00: A geochronological toolkit for Microsoft Excel. California: Berkeley Geochronology Center.

Mao, X.C., Wang, L.Q., Li, B., Wang, B.D., Wang, D.B., Yin, F.G., and Sun, Z.M., 2012. Discovery of the Late Silurian volcanic rocks in the Dazhonghe area, Yunxian-Jinggu volcanic arc belt, western Yunnan, China and its geological significance. Acta Petrologica Sinica, 28 (5): 1517–1528 (in Chinese with English abstract).

McLennan, S.M., Hemming, S., McDaniel, D.K., and Hanson, G.N., 1993. Geochemical approaches to sedimentation, provenance, and tectonics. Special Paper of the Geological Society of America, 284: 21–40.

McLennan, S.M., Taylor, S.R., McCulloch, M.T., and Maynard, J.B., 1990. Geochemical and Nd–Sr isotopic composition of deep-sea turbidites: crustal evolution and platetectonic association. Geochimica et Cosmochimica Acta, 54: 2015–2050.

Nakano, N., Osanai, Y., Nam, V. N., and Tri, V.T., 2018. Bauxite to eclogite: Evidence for late Permian supracontinental subduction at the Red River shear zone, northern Vietnam. Lithos, (302–303): 37–49.

Nesbitt, H.W., and Young, G.M., 1982. Early Proterozoic climates and plate motions inferred from major element chemistry of lutites. Nature, 299: 715–717.

Nesbitt, H.W., and Young, G.M., 1984. Prediction of some weathering trends of plutonic and volcanic rocks based on thermodynamic and kinetic considerations. Geochimica et Cosmochimica Acta, 48: 1523–1534.

Nesbitt, H.W., and Young, G.M., 1989. Formation and Diagenesis of Weathering Profiles. The Journal of Geology, 97(2): 129–147.

Nie, X.M., Feng, Q.L., Qian, X., and Wang, Y.J., 2015. Magmatic record of Prototethyan evolution in SW Yunnan, China: Geochemical, zircon U–Pb geochronological and Lu–Hf isotopic evidence from the Huimin metavolcanic rocks in the southern Lancangjiang zone. Gondwana Research, 28: 757–768.

Qi, X.X., Santosh, M., Zhao, Y.H., Hu, Z.C., Zhang, C., Ji, F.B., and Wei, C., 2016. Mid-Neoproterozoic ridge subduction and magmatic evolution in the northeastern margin of the Indochina block: Evidence from geochronology and geochemistry of calc-alkaline plutons. Lithos, 248–251: 138–

152.
Qi, X.X., Santosh, M., Zhu, L.H., Zhao, Y.H., Hu, Z.C., Zhang, C., and Ji, F.B., 2014. Mid-Neoproterozoic arc magmatism in the northeastern margin of the Indochina block, SW China: Geochronological and petrogenetic constraints and implications for Gondwana assembly. Precambrian Research, 245: 207–224.
Qi, X.X., Zeng, L.S., Zhu, L.H., Hu, Z.C., and Hou, K.J., 2012. Zircon U–Pb and Lu–Hf isotopic systematics of the Daping plutonic rocks: Implications for the Neoproterozoic tectonic evolution of the northeastern margin of the Indochina block, Southwest China. Gondwana Research, 21(1): 180–193.
Roser, B.P., and Korsch, R.J., 1986. Determination of tectonic setting of sandstone–mudstone suites using SiO_2 content and K_2O/Na_2O ratio. Journal of Geology, 94(5): 635–650.
Ryan, K.M., and Williams, D.M., 2007. Testing the reliability of discrimination diagrams for determining the tectonic depositional environment of ancient sedimentary basins. Chemical Geology, 242(1–2): 103–125.
Tapponnier, P., Lacassin, R., Leloup, P.H., Schärer, U., Zhong, D.L., Liu, X.H., Ji, S.C., Zhang, L.S., and Zhong, J.Y., 1990. The Ailaoshan/Red River metamorphic belt: Tertiary left-lateral shear between lndochina and South China. Nature, 343 (6257), 431–437.
Tapponnier, P., Peltzer, G., Armijo, R., Dain, A.Y.L., and Cobbold, P., 1982. Propagating extrusion tectonics in Asia: new insights from simple experiments with plasticine. Geology, 10(12), 611–616.
Usuki, T., Lan, C.Y., Yui, T.F., Iizuka, Y., Vu, Van Tich, Tran, Tuan Anh, Okamoto, K., Wooden, J.L., and Liou, J.G., 2009. Early Paleozoic medium-pressure metamorphism in central Vietnam: evidence from SHRIMP U–Pb zircon ages. Geosciences Journal, 13(3): 245–256.
Verma, S.P., and Armstrong-Altrin, J.S., 2016. Geochemical discrimination of siliciclastic sediments from active and passive margin settings. Sedimentary Geology, 332: 1–12
Wang, D.B., Tang, Y., Liao, S.Y., Yin, F.G., Sun, Z.M., and Wang, L.Q., 2013. Zircon U-Pb dating and its geological implications of the metamorphic rock series in Ailaoshan Ranges, western Yunnan. Acta Petrologica Sinica, 29(4): 1261 –1278 (in Chinese with English abstract).
Wang, F., Liu, F.L., Liu, P.H., Shi, J.R., and Cai, J., 2016. Petrology, geochemistry, and metamorphic evolution of meta-sedimentary rocks in the Diancang Shan–Ailaoshan metamorphic complex, Southeastern Tibetan Plateau. Journal of Asian Earth Sciences, 124: 68–93.
Wang, J.G., Chen, D.Z., Yan, D.T., Wei, H.Y., and Xiang, L., 2012. Evolution from an anoxic to oxic deep ocean during the Ediacaran–Cambrian transition and implications for bioradiation. Chemical Geology, 306–307: 129–138.
Wang, Q.F., Deng, J., Li, C.S., Li, G.J., Yu, L., and Qiao, L., 2014. The boundary between the Simao and Yangtze blocks and their locations in Gondwana and Rodinia: Constraints from detrital and inherited zircons. Gondwana Research, 26 (2): 438–448.
Wang, W., Zeng, M.F., Zhou, M.F., Zhao, J.H., Zheng, J.P., and Lan, Z.F., 2018. Age, provenance and tectonic setting of Neoproterozoic to early Paleozoic sequences in southeastern South China Block: Constraints on its linkage to western Australia-East Antarctica. Precambrian Research, 309: 290–308.
Wang, Y.J., Qian, X., Cawood, P.A., Liu, H.C., Feng, Q.L., Zhao, G.C., Zhang, Y.H., He, H.Y., and Zhang, P.Z., 2017. Closure of the East Paleotethyan Ocean and amalgamation of the Eastern Cimmerian and Southeast Asia continental fragments. Earth-Science Reviews, 186: 195–230. doi.org/10.1016/j.earscirev.2017.09.013
Wang, Y.J., Zhang, A.M., Fan, W.M., Zhao, G.C., Zhang, G.W., Zhang, Y., Zhang, F.F., and Li, S.Z., 2011. Kwangsian crustal anatexis within the eastern South China Block: Geochemical, zircon U–Pb geochronological and Hf isotopic fingerprints from the gneissoid granites of Wugong and Wuyi–Yunkai Domains. Lithos, 127: 239–260.
Wang, Y.J., Zhang, F.F., Fan, W.M., Zhang, G.W., Chen, S.Y., Cawood, P.A., and Zhang, A.M., 2010. Tectonic setting of the South China Block in the early Paleozoic: resolving intracontinental and ocean closure models from detrital zircon U–Pb geochronology. Tectonics, 29(6): 1–16.
Wang, Y.J., Zhou, Y.Z., Cai, Y.F., Liu, H.C., Zhang, Y.Z., and Fan, W.M., 2016. Geochronological and geochemical constraints on the petrogenesis of the Ailaoshan granitic and migmatite rocks and its implications on Neoproterozoic subduction along the SW Yangtze Block. Precambrian Research, 283: 106–124.
Weltje, G.J., 2006. Ternary sandstone composition and provenance: an evaluation of the "Dickinson model". In: Buccianti, A., Mateu-Figueras, G., Pawlowsky-Gahn, V. (Eds.), Compositional Data Analysis in the Geosciences: From Theory to Practice: Geological Society of London. Special Publications, 264: 79–99.
Wiedenbeck, M., Alle, P., Corfu, F., Griffin, W.L., Meier, M., Oberli, F., von Quadt, A., Roddick, J.C., and Spiegel, W., 1995. Three natural zircon standards for U–Th–Pb, Lu–Hf, trace element and REE analyses. Geostandards News letters, 19: 1–23.
Wu, W.B., Liu, J.L., Chen, X.Y., and Zhang, L.S., 2017. Zircon U–Pb ages, Hf isotope data, and tectonic implications of Early –Middle Triassic granitoids in the Ailaoshan high-grade metamorphic belt of Southeast Tibet. International Journal of Earth Sciences, 106(3): 875–897.
Xia, X.P., Nie, X.S., Lai, C.K., Wang, Y.J., Long, X.P., and Meffre, S., 2016. Where was the Ailaoshan Ocean and when did it open: A perspective based on detrital zircon U–Pb age and Hf isotope evidence. Gondwana Research, 36: 488–502.
Xing, X.W., 2016. Early Paleozoic tectonic nature in SW Yunnan: constraints from magmatism and sedimentation. Beijing: The University of Chinese Academy of Sciences (Ph.D. thesis): 1–170 (in Chinese with English abstract).
Xu, Y.J., Cawood, P.A., Du, Y.S., Hu, L.S., Yu, W.C., Zhu, Y.H., and Li, W.C., 2013. Linking south China to northern Australia and India on the margin of Gondwana: Constraints from detrital zircon U-Pb and Hf isotopes in Cambrian strata. Tectonics, 32: 1547–1558.
Xu, Y.J., Du, Y.S., Cawood, P.A., Zhu, Y.H., Li, W.C., and Yu, W.C., 2012. Detrital zircon provenance of Upper Ordovician and Silurian strata in the northeastern Yangtze Block: Response to orogenesis in South China. Sedimentary Geology, 267–268: 63–72.
Yao, J.L., Shu, L.S., and Santosh, M., 2011. Detrital zircon U–Pb geochronology, Hf-isotopes and geochemistry — new clues for the Precambrian crustal evolution of Cathaysia Block, South China. Gondwana Research, 208-211: 553–567.
Yao, W.H., Li, Z.X., Li, W.X., Su, L., and Yang, J.h., 2015. Detrital provenance evolution of the Ediacaran–Silurian Nanhua foreland basin, South China. Gondwana Research, 28: 1449–1465.
Yao,W.h., Li, Z.X., Li, W.X., Li, X.H., and Yang, J.H., 2014. From Rodinia to Gondwanaland: a tale of detrital zircon provenance analyses from the southern Nanhua Basin, South China. American Journal of Science, 314: 278–313.
YGS (Yunnan Geological Survey), 1975. 1:200000 Scale Geological Map of Jinping-Hekou (unpublished map sheet and explanation notes).
YGS (Yunnan Geological Survey), 1976a. 1:200000 Scale Geological Map of Xinping (unpublished map sheet and explanation notes).
YGS (Yunnan Geological Survey), 1976b. 1:200000 Scale Geological Map of Mojiang (unpublished map sheet and explanation notes).
YGS (Yunnan Geological Survey), 1976c. 1:200000 Scale Geological Map of Yuanyang-Damalu (unpublished map sheet and explanation notes).
Zelazniewicz, A., Tran, H.T., and Larionov, A., 2013. The significance of geological and zircon age data derived from the wall rocks of the Ailaoshan-red River shear zone, NW Vietnam. Journal of Geodynamics, 69(3): 122–139.
Zhai, M.G., Cong, B.L.,Qiao, G.S., and Zhang, R.Y., 1990. Sm\Nd and Rb\Sr geochronology of metamorphic rocks from SW Yunnan orogenic zones, China. Acta Petrologica Sinica, 16(4): 1–11 (in Chinese with English abstract)

Zhang, B., Yin, C.Y., Zhang, J.J., Wang, J.M., Zhong, D.L., Wang, Y., Lai, Q.Z., Yue, Y.H., and Zhou, Q.Y., 2017. Midcrustal shearing and doming in a Cenozoic compressive setting along the Ailaoshan-Red River shear zone. Geochemistry Geophysics Geosystems, 18(1): 400–433.

Zhang, B., Zhang, J.J., Zhong, D.L., Yang, L.K., Yue, Y.H., and Yan, S.Y., 2012. Polystage deformation of the Gaoligong metamorphic zone: Structures, $^{40}Ar/^{39}Ar$ mica ages, and tectonic implications. Journal of Structural Geology, 37: 1–18.

Zhong, D.L., 1998. Paleotethysides in Western Yunnan and Sichuan, China. Beijing: Science Press, 1–235 (in Chinese).

Zhong, D.L., Tapponnier, P., Wu, H.W., Zhang, L.S., Ji, S.C., Zhong, J.Y., Liu, X.H., Schärer, U., Lacassiu, R., and Leloup, P., 1990. Large-scale strike-slip-fault-the major structure of intracontinental deformation after collision. Chinese Science Bulletin, 35(4): 304–309.

Zhou, M.F., Yan, D.P., Kennedy, A.K., Li, Y.Q., and Ding, J., 2002. SHRIMP U-Pb zircon geochronological and geochemical evidence for Neoproterozoic arc magmatism along the western margin of the Yangtze block, South China: Earth and Planetary Science Letters, 196(1–2): 51–67. doi:10.1016/S0012-821X(01)00595-7.

Zi, J.W., Cawood, P.A., Fan, W.M., Wang, Y.J., Tohver, E., McCuaig, T.C., and Peng, T.P., 2012. Triassic collision in the Paleo-Tethys Ocean constrained by volcanic activity in SW China. Lithos, 144–145: 145–160.

About the first and corresponding author

JI Lei, male, postdoctor of Chinese Academy of Geological Sciences, major: mineralogy, petrology, mineral deposit science, research direction: metamorphism and metamorphic chronology.